



## Review

## Review of recent trends in photoelectrocatalytic conversion of solar energy to electricity and hydrogen



Panagiotis Lianos

Department of Chemical Engineering, University of Patras, 26500 Patras, Greece

## ARTICLE INFO

## Article history:

Received 13 January 2017

Received in revised form 22 March 2017

Accepted 26 March 2017

Available online 28 March 2017

## Keywords:

Photoelectrocatalytic

Photoelectrochemical

Hydrogen

Water splitting

Photocatalytic fuel cells

## ABSTRACT

This work is a review of the recent trends in the photoelectrocatalytic conversion of solar energy into electricity or hydrogen. It focuses on photocatalytic fuel cells and photoelectrocatalytic water splitting systems and presents both the basic principles and the design of devices. It includes a broad review of materials employed for the construction of photoanodes, photocathodes and tandem cells and highlights the related research fields which are expected to be of interest in the near future. The review is intended to become a basic manual for new adepts to the field and at the same time a handy reference to experienced researchers.

© 2017 Elsevier B.V. All rights reserved.

## Contents

1. Introduction-photoelectrochemical cells .....	236
2. The standard structure and functionality of a photoelectrocatalysis cell .....	236
2.1. Fundamentals .....	236
2.2. Driving force for cell operation .....	238
2.3. Photoelectrocatalysis with photocathode electrodes .....	239
3. Recent trends in the study of semiconductors for photoanodes .....	239
3.1. Mesoporous titania as standard photocatalyst .....	239
3.2. WO <sub>3</sub> photoanodes .....	241
3.3. BiVO <sub>4</sub> photoanodes .....	242
3.4. Fe <sub>2</sub> O <sub>3</sub> photoanodes .....	243
4. Semiconductors for photocathodes .....	243
5. Choice of counter electrodes .....	244
5.1. Oxygen reduction electrocatalysts .....	244
5.2. Hydrogen evolution electrocatalysts .....	244
6. Choice of electrolytes .....	245
7. Selected topics related with PFC and WS operation .....	245
7.1. Tandem cells for photoelectrocatalytic operation .....	245
7.2. Current doubling .....	245
7.3. Calculation of cell efficiency .....	246
8. Collection of data from recent publications .....	247
8.1. Electricity production by photocatalytic fuel cells (PFCs) .....	247

**Abbreviations:** ALD, atomic layer deposition; CB, conduction band; CC, carbon cloth; CIGS, Cu(In,Ga)Se<sub>2</sub>; CZTS, Cu<sub>2</sub>ZnSnS<sub>4</sub>; DSSC, dye-sensitized solar cell; GO, graphene oxide; HEC, hydrogen evolution catalyst; OEC, oxygen evolution catalyst; PEC, photoelectrochemical; PFC, photocatalytic fuel cell or photo-fuel-cell; Pt/C, platinum-carbon electrocatalyst; PV, photovoltaic; QD, quantum dot; RGO, reduced graphene oxide; S, semiconductor; SSA, specific surface area; STH, solar to hydrogen efficiency; TNT, titania nano-tubes; VB, valence band; WS, water splitting.

E-mail address: [lianatos@upatras.gr](mailto:lianatos@upatras.gr)

8.2.	Hydrogen production by photoelectrocatalytic oxidation of organic substances .....	248
8.3.	Photoelectrocatalytic hydrogen production in the presence of inorganic sacrificial agents .....	248
8.4.	Water splitting processes.....	248
9.	Summary and perspectives.....	249
	References.....	250

## 1. Introduction-photoelectrochemical cells

The foundations of modern photoelectrochemistry are laid by the works of Brattain and Garrett and later of Gerischer [1–3]. The titles of their works may be used to define the term Photoelectrochemistry and Photoelectrochemical cells [1,2]. Thus Photoelectrochemical (PEC) cells are those cells the functionality of which is based on the behavior of the interface between a semiconductor and an electrolyte. In fact, photoelectrochemical cells were reported already in 1839 by Edmond Becquerel [4]. At that time and for several more decades, the interest was in photography. Becquerel and his contemporaries were interested in the study of silver halide colloidal dispersions and their photoactivity. Silver halide, a principal component of photographic materials is, of course, a semiconductor. Therefore, we might say that modern photoelectrochemistry is a child of photography [3]. The study of photoelectrochemical cells attained “explosive” dimensions after two seminal works, first by Fujishima and Honda [5] and later by O'Regan and Grätzel [6]. The great interest that these works have arisen may be associated with the energy crisis of the seventies when the World for the first time realized that the supply of fossil fuels cannot last forever and that humanity would have to face its geopolitical consequences. The above works then signaled the study of photoelectrochemical cells as inexpensive means of solar energy conversion thus highlighting the broad use of renewable energy resources. Indeed, solar energy can be converted into usable forms of energy by means of photoelectrochemical cells. PEC cells can be divided into two major categories: Regenerative solar cells,

which convert solar energy to electricity and Photosynthetic cells, which convert solar energy into solar fuels, principally, hydrogen. These two categories are each represented by the above two seminal works. Thus the work of Fujishima and Honda incited interest into photoelectrochemical water splitting (WS) [5] while the work of O'Regan and Grätzel focused on electricity production by means of the so-called dye-sensitized solar cells (DSSCs) [6]. PEC cells may still be divided into a third category, the Photocatalytic Fuel Cells or Photo-Fuel-Cells (PFCs), which photocatalytically degrade an organic substance to produce electricity. PFC origins are not so well marked as the previous categories since they are based on similar traits as the photosynthetic PEC cells. However, reference should be made to the work by M. Kaneko et al. where the term PFC was lancet for the first time [7] and where the idea of using biomass products and water-soluble wastes to photoelectrocatalytically produce electricity was highlighted. Since the term Photoelectrochemical refers to both Regenerative and Photosynthetic cells, another more specific term, Photoelectrocatalytic and Photoelectrocatalysis, is mainly used to distinguish processes associated with Photocatalytic Fuel Cell and Solar Fuel production systems. Photoelectrocatalysis is, of course, carried out in PEC cells and it is also based on the properties of semiconductor-electrolyte interface. The present work will focus on recent advances in Photoelectrocatalysis including Photocatalytic Fuel Cell (PFC) and Water Splitting (WS) processes.

## 2. The standard structure and functionality of a photoelectrocatalysis cell

### 2.1. Fundamentals

In its most common version, a PEC cell designed for photoelectrocatalysis purposes is assembled with the following components. Fig. 1 pictorially illustrates these components. A photoanode electrode carrying a nanostructured photocatalyst absorbs photons, which generate electron-hole pairs. Electrons are collected by the photoanode electrode and they are conducted through an external circuit to the cathode (counter) electrode, where they take part in reduction reactions facilitated by a nanostructured electrocatalyst. Photogenerated holes are consumed by oxidation reactions, for example oxidation of water or oxidation of water-soluble organic or inorganic substances. Both photoanode and cathode electrodes are in contact with an electrolyte, where the organic “fuel” and various ionic species are dissolved. The nature of these ionic species depends, among other factors, on the pH. Table 1 summarizes the principal oxidation reactions which are expected to take place in a photoelectrocatalysis cell which carries a photoresponsive anode (photoanode) [8–10].

Table 1 lists the electrochemical potential for water oxidation at two pH extremes. In the case of  $C_xH_yO_z$ -type compounds, oxidation potential will, of course, vary from one substance to the other. In addition, oxidation of such substances takes place by a series of steps, according to its complexity. For example, for ethanol the following mineralization scheme prevails: ethanol  $\rightarrow$  acetaldehyde  $\rightarrow$  acetic acid  $\rightarrow$   $CO_2 + H_2O$ . Therefore, the oxidation potential is specific for each reaction type and can be calculated by following a standard protocol. Examples can be found in Refs. [9,10]. For the case of inorganic sacrificial agents,

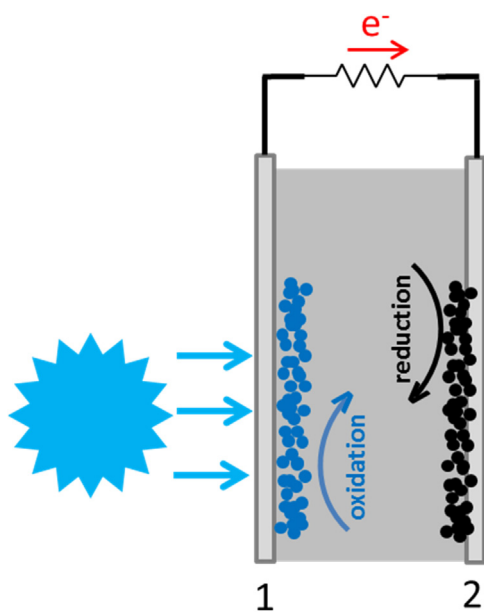


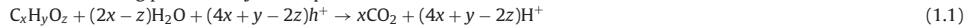
**Fig. 1.** Schematic representation of a photoelectrocatalysis cell composed of a transparent photoanode electrode carrying a nanostructured photocatalyst (1) and a cathode (counter) electrode carrying a nanostructured electrocatalyst (2). The transparent photoanode plays the role of reactor window. Photogenerated electrons are conducted through the external circuit and carry out reduction reactions at the cathode while photogenerated holes are consumed by oxidation reactions at the photoanode.

**Table 1**

Standard oxidation reactions involving organic fuel and water, taking place at the photoanode electrode.

- The nanostructured photocatalyst is a semiconductor S in contact with the electrolyte.
- Absorption of photons generates electrons and holes  $S + h\nu \rightarrow S(e^- + h^+)$
- Most photogenerated electrons, which escape recombination, flow in the external circuit. Some may interact with  $O_2$ , if present, producing superoxide and finally hydroxyl radicals.
- Those photogenerated holes, which escape recombination, interact with the fuel or water by the following principal reaction schemes. The fuel is represented by  $C_xH_yO_z$ -type compounds (alcohols, organic acids, carbohydrates), since they are the best fuel both for electricity and hydrogen production:

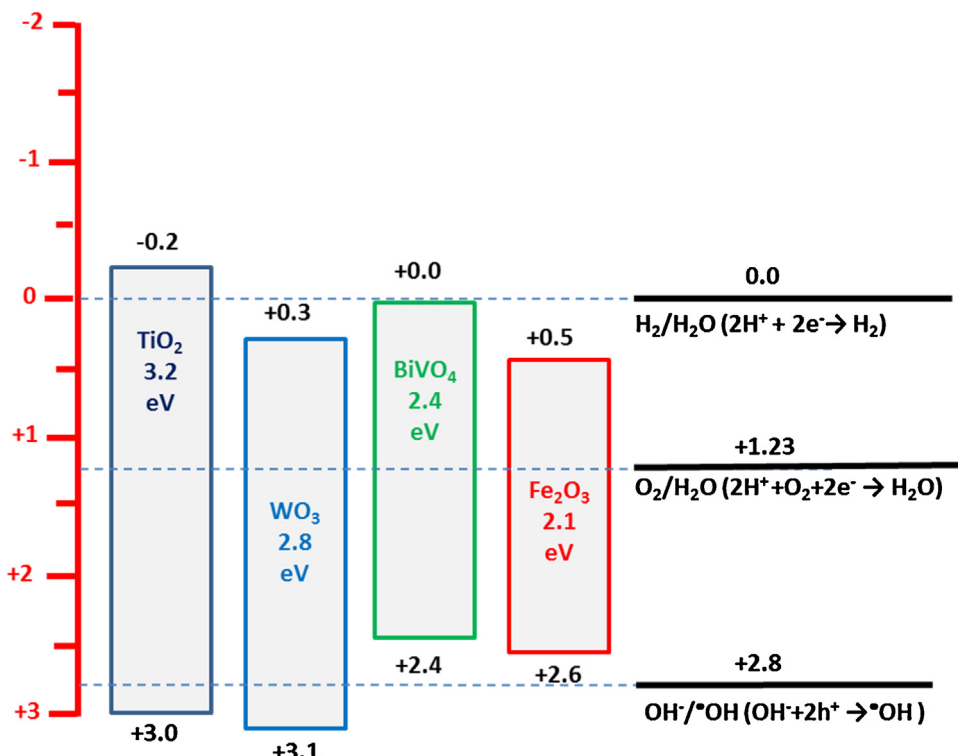
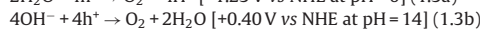
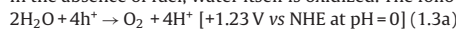
Oxidation taking place mainly at low pH



Oxidation taking place mainly at high pH



In the absence of fuel, water itself is oxidized. The following two reactions correspond to two pH extremes.

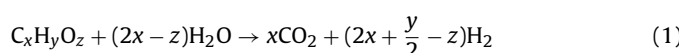


### Values vs SHE

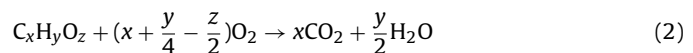
**Fig. 2.** Energy states and band gap energies of a few popular oxide semiconductor photocatalysts and of the reduction levels in the absence and in the presence of oxygen. The oxidation level for the production of hydroxyl radicals is also shown. All values are expressed vs SHE (corresponding to pH 0).

**Table 2** provides some characteristic examples of oxidation reactions [7,10–14].

Oxidation half reactions at the photoanode are balanced by reduction half reactions at the cathode. These latter reactions do not in principle depend on the kind of organic fuel or inorganic sacrificial agent but they are standard reactions affected only by the pH and the presence or absence of  $O_2$ , as seen in **Table 3** [8–10]. Thus oxidation Reaction (1.2b) (**Table 1**) is balanced either by Reactions (3.2) or (3.4) (**Table 3**), depending on whether it is carried out in inert environment or in the presence of oxygen. In the first case the overall reaction becomes [10]



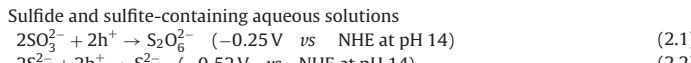
and it corresponds to (photoelectrocatalytic) reforming for hydrogen production [15,16] while in the presence of oxygen it becomes



and it corresponds to (photoelectrocatalytic) fuel oxidation and mineralization. In all cases, cell function depends on the flow of electrons in the external circuit. Oxidation then of an organic fuel, or an inorganic sacrificial agent or water itself leads to current flow and hydrogen production in an inert environment while in the presence of oxygen only electricity is produced. As it will become clear below, since in most studied cases hydrogen is produced under applied external electric bias, it makes no practical sense to talk about simultaneous production of hydrogen and electricity. Electricity is practically produced only in the presence of oxygen.

**Table 2**

Examples of oxidation reactions taking place at the photoanode electrode and involving inorganic sacrificial agents.



Ammonia-containing aqueous solution

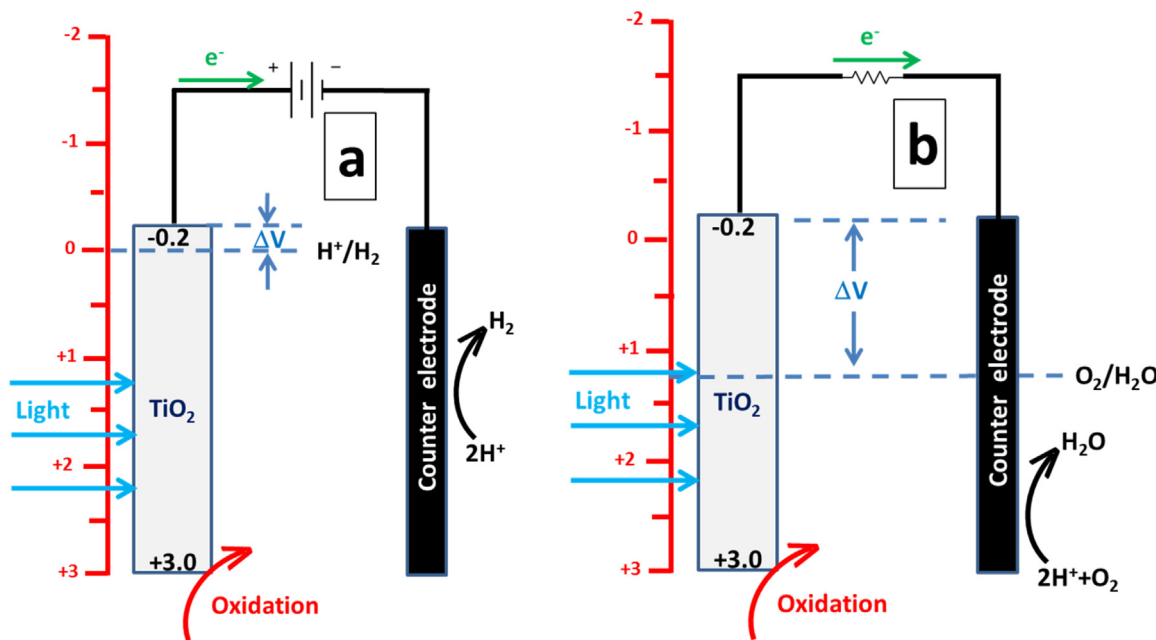
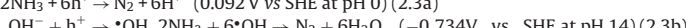
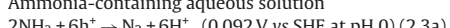
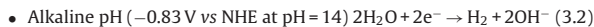
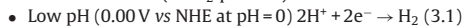


**Fig. 3.** Schematic illustration of a photoelectrocatalysis cell operating under external electric bias and producing hydrogen (a) and operating without bias, producing electricity (b). The energy levels of the photocatalyst correspond to open-circuit values, i.e. before establishing electric circuit connections.

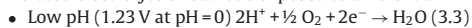
**Table 3**

Standard reduction reactions taking place at the cathode electrode.

Inert environment (no O<sub>2</sub> present)



Aerated electrolyte or cathode exposed to ambient air



Exception to this rule constitute unassisted tandem cells, which will be discussed in Section 7.1.

## 2.2. Driving force for cell operation

The driving force that leads electrons from the photoanode to the cathode electrode depends on the potential difference between the Fermi levels of the two electrodes. For practical purposes, cell function can be understood to a good approximation by the following approach. For n-type semiconductor photocatalysts, the photoanode potential is close to the potential of the conduction band (CB) of the semiconductor. The cathode electrode potential, in the presence of an appropriate electrocatalyst which is expected to eliminate overpotential developing between the electrode and the electrolyte, should be approximately equal to the redox potential of the reduction reaction. Therefore, the driving force is analogous

to the difference between the CB of the photocatalyst and the redox potential of the reduction reaction.

Fig. 2 illustrates the CB and VB (valence band) levels of a few popular semiconductor photocatalysts in contrast with reduction potentials in aqueous environment. The shown photocatalysts have a CB which is slightly more negative (TiO<sub>2</sub>), equal (BiVO<sub>4</sub>) or even more positive (WO<sub>3</sub> or Fe<sub>2</sub>O<sub>3</sub>) than hydrogen production level. Even in the case of titania, the favorable difference is eliminated by inevitable losses. Therefore, electrons can hardly flow from the photoanode to cathode electrode unless an external bias is applied. For this reason, photoelectrocatalytic hydrogen production is realized only under external bias, as shown in Fig. 3a. On the contrary, if the cathode electrode is aerated, then oxygen may be reduced at a potential which is as positive as 1.23 V vs SHE. The difference of this level is large enough (for example, for titania it is about 1.4 V) to allow the cell to run without bias (cf. Fig. 3b). In that case, the cell produces electric power with high open-circuit voltage [17].

The photocatalysts depicted in Fig. 2 have valence bands which are oxidative enough to carry out many oxidation reactions. The most important of all is the formation of hydroxyl radicals. As seen in Fig. 2, only two of the illustrated photocatalysts are capable of producing hydroxyl radicals. Oxidation reactions are facilitated by hydroxyl radicals since the target molecules are in the bulk solution and only a limited number may be attached on the photocatalyst surface to allow direct electron transfer to the VB (i.e. direct oxidation). Therefore, among the above four photocatalysts TiO<sub>2</sub> and WO<sub>3</sub> can effectively function in a PFC and produce electricity (cf. Fig. 3b). In other words, for PFC operation, TiO<sub>2</sub> and WO<sub>3</sub> have a CB which is more negative than the oxygen reduction level, therefore, they can function without bias, and have a VB which is more

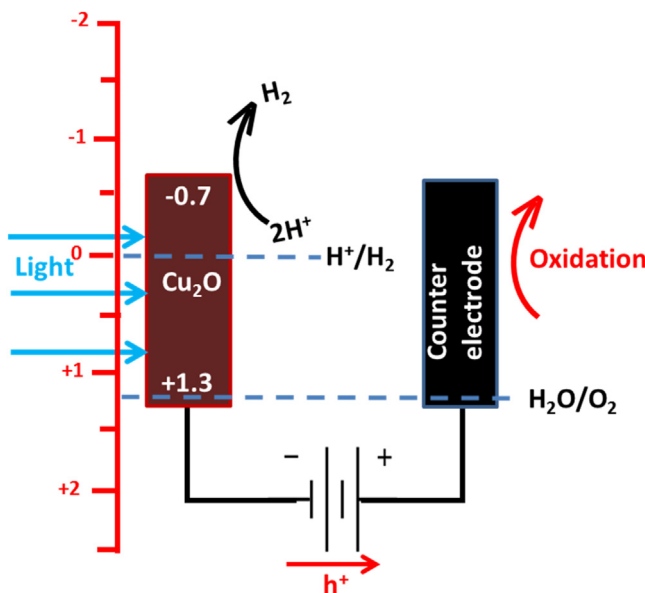


**Fig. 4.** Schematic illustration of a photoelectrocatalysis cell operating with a Cu<sub>2</sub>O photocathode. The illustrated redox reactions refer to low pH. At high pH, reactions are modified according to Table 3.

positive than the hydroxyl radical formation level, and therefore, they can efficiently oxidize any organic fuel. Nevertheless, oxidative capacity towards organic substances albeit of lower extent has also been observed with the other two photocatalysts as will be discussed later.

### 2.3. Photoelectrocatalysis with photocathode electrodes

The ideal photoelectrocatalysis cell should comprise a photo-electrode carrying a photocatalyst having CB and VB levels that straddle the water reduction and water oxidation potentials (0 and 1.23 V vs SHE, respectively), *i.e.*, where the CB has sufficiently negative potential and the VB is sufficiently more positive than 1.23 V. TiO<sub>2</sub> and the rest of the photocatalysts of Fig. 2 have sufficiently positive VBs, as already said. However only TiO<sub>2</sub> has a negative CB, which is in practice eliminated by losses. There are other photocatalysts which do straddle water reduction and oxidation potentials. For example, SrTiO<sub>3</sub> and LaTi<sub>2</sub>O<sub>7</sub> [18–20], CdS [3,18,20,21] and others. However, these semiconductors suffer of either low charge carrier mobility and high recombination rates or they are very unstable. For this reason, even though, some of them like CdS have been extensively studied, they have practically been abandoned. One way to solve the low electronegativity of the CB of standard oxide photocatalysts is to employ p-type semiconductors, deposited on the cathode electrode, which thus function as photocathode. The anode electrode may then carry an n-type photocatalyst or simply carry an electrocatalyst. The function of such a cell is schematically illustrated in Fig. 4 [21–23]. In this figure, Cu<sub>2</sub>O has been chosen as p-type semiconductor photocatalyst. This is a standard choice, even though it also suffers of low stability. Measures which have been taken to deal with stability issues will be discussed later. In Fig. 4, light absorption by the photocathode creates electrons and holes. Electrons in the CB are at a level which is negative enough to promote water reduction and hydrogen gas production. The photogenerated holes are transferred by the external circuit to the counter electrode (anode) facilitating oxidation reactions, for example water oxidation. However, Cu<sub>2</sub>O has a VB which is too close to the water oxidation level, 1.3 V vs 1.23 V. Therefore there is not enough drive to lead holes to the counter electrode. There are various approaches to solve this problem. For example,

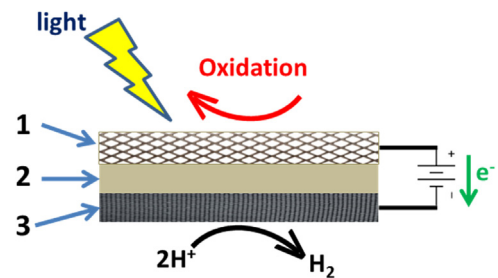


**Fig. 5.** Schematic illustration of a membrane electrode assembly for PFC or WS operation: (1) porous photoanode electrode; (2) ion transfer membrane; and (3) porous cathode electrode. Oxidation reaction could be carried out in aqueous or gaseous phase and could involve an organic fuel or pure water. Reduction could be also carried out in aqueous or gaseous phase and could involve not only proton (as illustrated) but also water or oxygen reduction.

apply an external bias, as shown in Fig. 4 or combine the photocathode with a photoanode. Related examples will be given in Section 7.1. The choice of a photocathode has the advantage that p-type semiconductors usually have a low band gap, therefore they absorb light in a substantial portion of the Visible and near IR. In addition, p-type semiconductors do not suffer of self-oxidation problems as it happens with several n-type semiconductors (for example, CdS, ZnS, ZnO, etc.).

## 3. Recent trends in the study of semiconductors for photoanodes

### 3.1. Mesoporous titania as standard photocatalyst

Mesoporous nanocrystalline anatase (TiO<sub>2</sub>) remains the best choice for the construction of photoanodes, not only for PFC and WS operation but for all kinds of photoelectrochemical cells. There has been a lot of effort to synthesize mesoporous titania in the form of one-dimensional nanostructures (nanorods, nanotubes, nanowires, *etc.*) by addressing the possibility that electron-hole recombination may have lower chances in low dimensionality nanostructures. In addition, low dimensionality nanostructures may increase specific surface area (SSA) of the photocatalyst. However, all factors taken into account it seems that nanoparticulate titania has no rival. The reason is that low dimensionality nanostructures are good if they are really made without defects. This is very difficult to realize while it is less important in the case of nanoparticles. Nevertheless, synthesis and deposition of titania in one-dimensional nanostructures remains and apparently will remain a very popular subject.

Titania nanotubes (TNT) have been frequently studied in association with water splitting processes [24,25]. Among other advantages, TNTs are formed on metal substrates, which can directly serve as electrodes. Thus in a recent version of a WS device employing a membrane-electrode assembly, TNTs were formed by electrochemical anodization on a Ti-web of microfibers, which served as photoanode [26]. When the anode and cathode electrodes are placed in a short distance between each other, separated only by an ion transfer membrane then the membrane plays both the role of separator and electrolyte. Because of the short distance between the electrodes, the internal resistance decreases and thus the current density and subsequently the cell efficiency increases. This configuration is schematically represented by Fig. 5. The prerequisite of such a design is that both photoanode and cathode electrodes are porous and allow diffusion of ionic and gaseous species through them. As it will be discussed later, porous cathodes can be obtained by using, for example, carbon cloth. In Ref. [26], a porous photoanode was obtained by using a Ti-web of metal microfibers on which TNT were grown by anodization. Such a photoanode can be

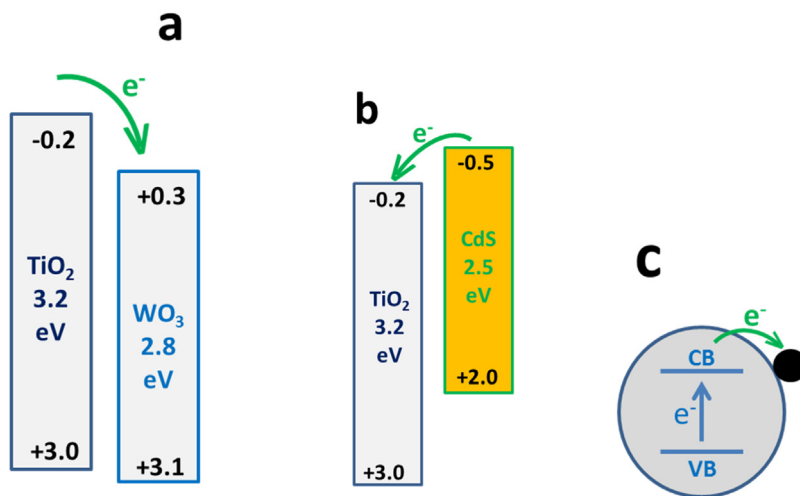


**Fig. 6.** Schematic illustration of charge carrier separation by injection of an electron in the CB of one semiconductor into the lower-lying CB of a second semiconductor (a,b) or a metal co-catalyst (c). Similar charge separation may be achieved by corresponding hole injection. Sensitization of a large band gap semiconductor by a visible-light-absorbing small band gap semiconductor is also illustrated by (b).

additionally used to photocatalytically oxidize a gaseous fuel, be it organic material or water vapor [26,27].

As far as nanoparticulate titania films are concerned, it is essential to deposit them with very good crystallinity and very high specific surface area. The literature on titania is huge and the related information is summarized in a large number of review papers. In the present publication we will make a short reference to some very recent works. Increase of SSA has a direct beneficial effect on PEC cell efficiency. For example, the synthesis of titania by flame spray pyrolysis gave a product with SSA as high as  $249 \text{ m}^2 \text{ g}^{-1}$  [28,29]. In comparison, common titania P25 has a SSA of only  $50 \text{ m}^2 \text{ g}^{-1}$ . By making photoanodes with flame-spray-pyrolysis-synthesized titania the photocurrent was doubled compared to photoanodes made of titania P-25 [29]. Increase of SSA is, of course, very important but a different aspect of titania nanocrystals seems to be recently given increased weight. This is related to facet dependent photoactivity of shape-controlled anatase  $\text{TiO}_2$  [30]. In other words, crystal morphology and the effort to control crystal morphology emerges as an important tool for increasing titania photoactivity.

Titania has good charge transport properties, better than other popular oxide semiconductors. Its hole diffusion length is of the order of  $10^4 \text{ nm}$ , much larger than  $\text{WO}_3$  ( $\sim 150 \text{ nm}$ ) and hematite ( $2\text{--}4 \text{ nm}$ ) [31]. However, it still suffers of extensive electron-hole recombination. One way to limit this deficiency is to introduce graphene into the titania nanostructure. Graphene has very high electron mobility,  $2.5 \times 10^5 \text{ cm}^2 \text{ V}^{-1} \text{ s}^{-1}$ , about 100 times higher than that of silicon [32]. Introduction then of graphene creates electron “highways”, which support electron-hole separation. In addition, introduction of graphene, including graphene oxide (GO) and reduced graphene oxide (RGO) increases active surface area and introduces active photocatalytic sites [33–35]. Another way to limit electron-hole recombination is to associate titania with other semiconductor nanoparticles or metal co-catalysts. As seen in Fig. 6, when two species of different band levels come in contact, photo-generated charge carriers in one species may be injected to the other due to favorably lying energy states, thus achieving charge separation. This is also the basis of photosensitization. Indeed, combination of  $\text{TiO}_2$  with  $\text{WO}_3$  produced more efficient photocatalysts than each semiconductor alone [36]. Combination of titania with noble metal nanoparticles is the basis of photocatalytic hydrogen production but such combinations have been also applied to photoelectrocatalytic processes [37,38]. The presence of metal deposits on titania is also associated with plasmon resonance phenomena [39].

The most serious disadvantage of titania is its exclusive light-absorption in the UV. For this reason, efforts have been made to combine titania with various visible-light absorbing sensitizers. The literature on titania sensitizers is very rich, however, it mostly applies to DSSCs and other types of liquid electrolyte and solid-state solar cells. On the contrary, sensitization in aqueous environment faces many constraints and many stability issues. Metal sulfide quantum dots (QDs) are the most effective titania sensitizers. They are easy to synthesize and incorporate into the mesoporous titania structure by simple chemical processes, for example, the SILAR method (Successive Ionic Layer Adsorption and Reaction) [40,41]. Metal sulfides, for example  $\text{CdS}$  and  $\text{CdSe}$ , are n-type semiconductors and they are vulnerable to self-oxidation by VB holes. Therefore, their stability depends on fast scavenging of photogenerated holes by effective electron donors. This has been successful in WS cases being carried out in the presence of sulfur-containing inorganic sacrificial agents, the most popular being sulfide-sulfite combinations (cf. reactions in Table 2). Some other limited cases are also applicable. First rule is that the titania/sensitizer combined photocatalyst should have the capacity to carry out oxidation reactions. This is illustrated in Fig. 7, which shows energy diagrams for a mesoporous titania film,  $\text{CdS}$  and  $\text{CdSe}$  QDs and a few redox levels. It has been found that  $\text{CdS}$  deposited by the SILAR method on mesoporous titania forms nanoparticles that largely vary in size and optoelectronic properties [41]. For this reason, the diagram of Fig. 7, in the case of  $\text{CdS}$  shows a range of energy levels and not discrete values. It is seen that both  $\text{CdS}$  and  $\text{CdSe}$  have VB levels which can oxidize both sulfide as well as sulfite species (not shown but presented in Table 2). Therefore, sulfide/sulfite sacrificial agents function very well with  $\text{CdS}$  and  $\text{CdSe}$  (as well as with other metal sulfide) sensitizers of titania [11,42–44]. When however it comes to organic fuels which mostly necessitate the activation of hydroxyl radicals, only a limited number of QDs is functional. It has been thus found that only certain  $\text{CdS}$  and  $\text{ZnSe}$  species have this quality [41,44].

Titania may be sensitized by other agents beside metal sulfides. For example, graphene quantum dots have been recently shown to apply in combination with titania to photoelectrochemical WS [45]. There are reports which deal even with dye sensitization [46], even though, dyes are not considered to be stable sensitizers in aqueous environment. Even though, sensitization of titania for WS and PFC operation as well as for photocatalytic degradation purposes is the longest in time and the most widely studied related research field, the results are rather meager. For this reason, the search for lower

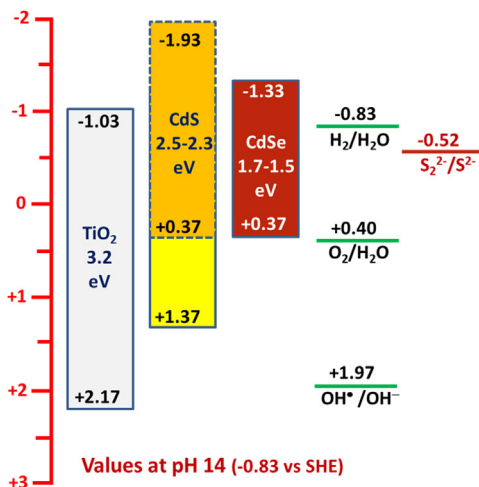


**Fig. 7.** Energy diagram of  $\text{TiO}_2$ ,  $\text{CdS}$  and  $\text{CdSe}$  quantum dots and a few redox levels applying to PFC and WS processes. The energy levels of  $\text{CdS}$  were obtained from Ref. [41] and their dispersion illustrates the fact that its optoelectronic properties and subsequently its photocatalytic properties depend on its synthesis and deposition method.

band gap semiconductor photocatalysts absorbing visible light is the current most active field of research.

In this respect, we should mention a large family of titanium-based ternary metal oxides, like  $\text{SrTiO}_3$  and  $\text{LaTi}_2\text{O}_7$  as well as non-metal doped titania, for example,  $\text{N}: \text{TiO}_2$ . These materials are principally studied for photocatalytic and less for photoelectrocatalytic applications. Many of them are characterized by visible light absorption, since they create energy states within the titania band gap thus making possible absorption of longer wavelength photons. However, most of them are less efficient photocatalysts than pure titania. These materials will not make subject of the present review but they may be found in several other publications [47–50].

### 3.2. $\text{WO}_3$ photoanodes

$\text{WO}_3$  is one of the most popular metal oxide semiconductor photocatalysts. It is being studied for several decades [51–54] as an alternative to the UVA absorbing titania.  $\text{WO}_3$  has a bandgap of 2.5–2.8 eV, therefore, it absorbs visible light up to 500 nm, which accounts for 12% of the solar radiation on the surface of the earth [54].  $\text{WO}_3$  is an n-type indirect semiconductor. It is relatively easy to synthesize and deposit on electrodes, it has a moderate hole-diffusion length ( $\sim 150$  nm [54]), it exhibits resistance against photocorrosion and it demonstrates satisfactory chemical stability at relatively low pH values. For this reason,  $\text{WO}_3$  has been studied as a photoanode material for photoelectrochemical water splitting applications [31,51–61]. Its valence band is located approximately at +2.8–3.1 V vs SHE, therefore, it is well placed for water oxidation and hydroxyl radical formation (cf. Fig. 2). Its conduction band is located at positive potentials (approximately +0.2 to +0.3 V vs SHE), therefore, a bias is necessary in order to guide photogenerated electrons to the counter electrode and produce hydrogen by water or proton reduction. The expected theoretical solar to hydrogen efficiency for  $\text{WO}_3$  photoanodes is about 4.8%, based on its range of light absorption [31] (the corresponding value is only 2.2% for titania [31]). Most of the works which study  $\text{WO}_3$  as photoanode material focus on water splitting applications. However, it is a matter of fact that when a sacrificial agent is introduced in water, for example an organic substance which may as well be an organic waste, the photocurrent produced by  $\text{WO}_3$  photoanodes is substantially enhanced [61]. This matter has been given less attention since the research community is mainly focused on purely water-

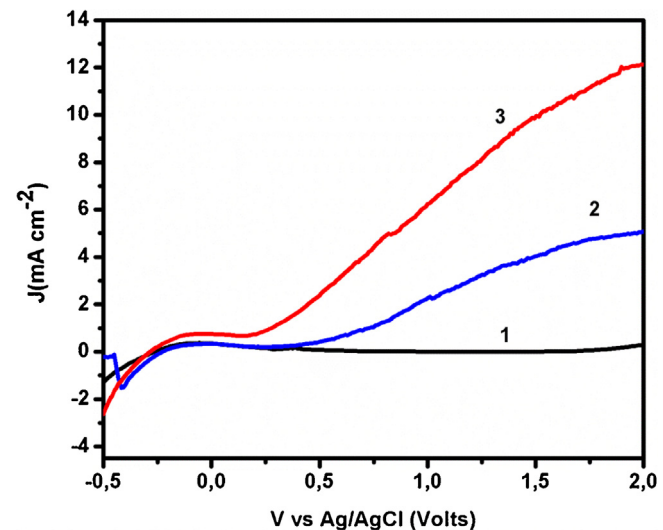


**Fig. 8.** JV curves recorded by using a 3-electrode cell comprising a  $\text{WO}_3$  photoanode, a Pt foil as counter electrode,  $\text{Ag}/\text{AgCl}$  as reference and 0.5 aqueous  $\text{NaClO}_4$  as electrolyte. The size of the photoanode was  $1 \text{ cm}^2$ : (1) curve recorded in the dark; (2) photocurrent recorded in the absence of added fuel; and (3) in the presence of 6.3% w/w ethanol (cf. Ref. [61]).

splitting applications. Increase of the current in the presence, for example, of ethanol can be seen in the following Fig. 8.

The current density, which was observed under bias in the absence of a sacrificial agent was doubled in the presence of ethanol. Increase of the current can be the result of enhanced hole scavenging in the presence of an electron donor, however, in a cell functioning under forward bias this factor is of smaller importance compared to current doubling phenomena. Current doubling originates from the formation of unstable radicals by oxidation of the sacrificial agent and the injection of extra electrons into the conduction band of the semiconductor photocatalyst [53,62–65]. More on this issue will be discussed in Section 7.2. Fig. 8 then verifies that the current flowing in the cell is higher in the presence of a sacrificial agent and, since hydrogen production rate is proportional to the current, hydrogen production is expected to increase in that case. This is verified by the data presented in Ref. [61], while corresponding data concerning the use of glucose as sacrificial agent can be found in Ref. [66].

Several comprehensive reviews on synthesis, properties and photoelectrochemical applications of  $\text{WO}_3$  can be found in Refs. [55,56,67]. A “classical” chemical approach for making  $\text{WO}_3$  photoanodes is given in [61] while formation of  $\text{WO}_3$  films by electrodeposition is reviewed in [55]. Recent examples on the study of  $\text{WO}_3$  photoanodes can be found in Refs. [59–61,68–71]. Many of the recent works are characterized by the effort to improve the quality of  $\text{WO}_3$  photoanodes by modifying synthesis and deposition procedures. Interestingly, among the highest currents reported are those found in [61]. Even though as already said,  $\text{WO}_3$  VB is sufficiently positive to justify water oxidation or hydroxyl radical formation, in practice, transfer of holes to the target in solution is not easy and this leads to great losses by electron-hole recombination. In other words, oxygen evolution is characterized by slow kinetics and large overpotential [72]. One strategy to limit this problem is to introduce mediators of photogenerated hole transfer, the so-called oxygen evolution catalysts which facilitate water oxidation and oxygen evolution [57,58,73]. In the case of  $\text{WO}_3$  which is stable only in low pH environments, it is necessary to deal with catalysts that are functional in acidic environment. Thus, for example, in Ref. [58], Keggin-type polyoxometalates were proposed for this purpose. Care should be also taken that their deposition will not

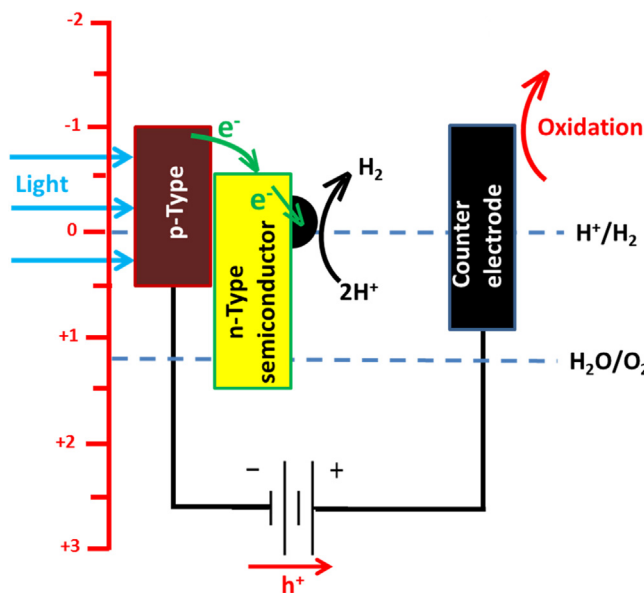


**Fig. 9.** Schematic illustration of a photoelectrocatalysis cell operating with a photocathode carrying a p-type semiconductor, a layer of an n-type semiconductor and a co-catalyst on the top. This combination provides a cascade transfer of electrons while n-type semiconductor additionally offers protection against corrosion and photo-corrosion. Cascade electron transfer diminishes overpotential for proton reduction.

obscure  $WO_3$  film. For example, in [72] a transparent nanoparticulate  $FeOOH$  has been proposed for this purpose. In this respect, we should underline the fact that in the presence of a sacrificial agent, like an organic substance dissolved in the liquid phase, there is no question of oxygen evolution, thus reforming of the organic substance, *i.e.* Reactions (1.1) and (1) can facilitate hydrogen evolution procedure.

In conclusion, nanoparticulate  $WO_3$  can be used for photoelectrocatalytic hydrogen production, preferably in the presence of organic fuel, in the same way as titania. Its advantage vs titania is its substantial visible light absorption. This is translated by higher current densities and higher hydrogen production rates [61]. Disadvantages with respect to titania are its lower stability, favored only in acidic electrolytes and the fact that  $WO_3$  films have lower SSA than most titania films.

### 3.3. $BiVO_4$ photoanodes

$BiVO_4$  is a medium band gap semiconductor, which has attracted attention as a visible light responsive photocatalyst for water splitting applications [54]. The most common and the only active polymorph of  $BiVO_4$  takes a monoclinic scheelite-like crystalline structure with a band gap of 2.4 eV (cf. Fig. 2). Bismuth vanadate is a stable non-toxic yellow pigment and it is preferred from the similarly-colored  $CdS$ , which is toxic and easily photo-corroded.  $BiVO_4$  conduction and valence band edges consist of vanadium 3d orbitals and a hybridization between oxygen 2p and bismuth 6s orbitals [54]. Its visible light absorption is related with bismuth 6s and vanadium 3d electron lone pairs, being located at relatively positive potentials [54]. Monoclinic  $BiVO_4$  was first developed by Kudo et al. [74] as water decomposition photocatalyst and has ever since been one of the most popular visible light responsive photocatalysts [54,74–81]. In 2003, Sayama et al. reported an IPCE value for photoelectrochemical water decomposition of 29% at 420 nm and by applying a bias of 1.9 V vs RHE [75]. More recently, Jie et al. attained a IPCE value of 73% at 420 nm by applying a bias of 1 V vs Ag/AgCl [76]. As a matter of fact, a bias is always necessary

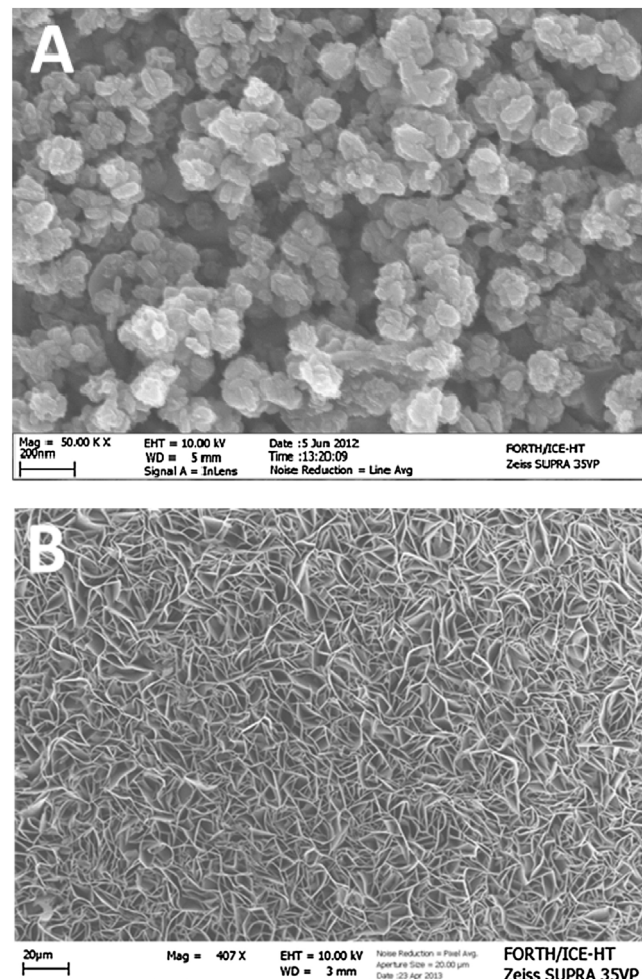


**Fig. 10.** SEM images of a  $CuS$  (A) and a  $Cu_2S$  (B) film. The scale bars are 200 nm and 20  $\mu m$ , respectively.

to obtain a substantial photocurrent by using  $BiVO_4$  photoanodes, apparently, because electron-hole recombination is very important in this material. A broad list of obtained photocurrents under various applied bias and  $BiVO_4$  structures as well as a broad account of various synthesis methods is given in the comprehensive review of Ref [80].

The maximum theoretical Solar-to-Hydrogen (STH) efficiency for monoclinic  $BiVO_4$  of  $E_g = 2.4$  eV is 9.1% [79,80], therefore, it is in principle a very promising photocatalyst. It is reminded that the corresponding percentages for  $WO_3$  and  $TiO_2$  are 4.8% and 2.2%, respectively [31]. However, the actual efficiencies obtained with pure  $BiVO_4$  are much lower [82] and the reason is low charge mobility and extensive electron-hole recombination. In order then to improve the photoelectrocatalytic data of  $BiVO_4$  photoanodes for water splitting applications,  $BiVO_4$  is frequently studied in the presence of metal dopants [80,83–87]. Metal dopants, are expected to modify the band structure and electronic properties of the ensuing material and result in increasing photocurrent. The term “dopant” is presently used in the sense of impurity, in fact, electron donor impurity. Charge carrier diffusion length in  $BiVO_4$  is difficult to measure. Nevertheless, in the presence of Mo as donor impurity, hole diffusion length was estimated to be  $\sim 100$  nm [88] while in another case by introducing Mo it was estimated to have changed from 47 to 183 nm [86]. In other words, metal dopants bring about a significant improvement of the electronic properties of bismuth

vanadate. Thus, for example, addition of Nb(V) tripled current density in a WS device functioning with sodium bicarbonate electrolyte [84].

Another approach to enhance BiVO<sub>4</sub> photoanode performance is to apply oxygen evolution catalysts, as in the case of WO<sub>3</sub>. Some notable examples may be found in Refs. [89–91]. When cobalt phosphate (Co-Pi), FeOOH or NiOOH, which are typical examples of oxygen evolution catalysts, are applied on BiVO<sub>4</sub>, they hamper surface recombination and decrease oxygen evolution overpotential. Thus in the case of Ref. [91], addition of combined FeOOH/NiOOH catalyst resulted in an impressive increase of the photocurrent.

Similarly to the case of WO<sub>3</sub>, BiVO<sub>4</sub> photoanodes have rarely been used for PFC operation in the presence of organic fuel. In addition, BiVO<sub>4</sub> has then been combined with other metal oxide photocatalysts [92,93]. It is obvious that this remains an unexplored and, at the same time, an interesting subject of research.

#### 3.4. Fe<sub>2</sub>O<sub>3</sub> photoanodes

Hematite ( $\alpha$ -Fe<sub>2</sub>O<sub>3</sub>) is another popular photocatalyst [80,94–97]. Its popularity stems from its visible light absorption, its relatively good efficiency and the easiness of its synthesis and application on electrodes. Hematite is stable in a wide pH range [98], it is considered to be non-toxic while it is very cheap since iron is one of the most abundant elements in the earth's crust (4th most abundant element) [94]. With a band gap of about 2.0 eV, it can absorb light beyond 600 nm, therefore, its theoretical Solar to Hydrogen Efficiency (SHE) is >15% [80] while the expected current density can reach 14 mA cm<sup>-2</sup> [80,97]. These advantages make hematite a very promising material. However, the expected efficiencies have actually never been achieved because hematite also carries some important disadvantages. For example, it suffers from low conductivity and fast recombination due to large effective mass of its charge carriers. Thus, while for TiO<sub>2</sub> and WO<sub>3</sub> the hole diffusion length is  $\sim$ 100  $\mu$ m and 100–150 nm, respectively, in the case of hematite it is only 2–4 nm [98]. Furthermore, electron mobility in hematite is low ( $10^{-1}$  V<sup>-1</sup> s<sup>-1</sup>) [99] and its excited state life time is short [100]. For this reason, it is necessary to apply hematite on electrodes in the form of thin films, in order to allow charge carriers to reach the electrode. However, hematite extinction coefficient is also low, therefore, the film must not be too thin, and thus a crucial film thickness optimization procedure should be put into effect. Finally, hematite conduction band (CB) is located around +0.4 V while its valence band (VB) lies around +2.5 V vs NHE [101]. Since then they do not straddle water reduction-oxidation potentials (0–1.23 V vs SHE), a hematite photoanode may be good for water oxidation but a bias is necessary for water reduction. This rich combination of advantages and disadvantages has created an intense effort for the optimization of film deposition procedures and subsequently, for the construction of efficient hematite photoanodes [102].

Hematite photoanodes have been made by several different procedures, among them, three being the most remarkable. Thus most efficient hematite photoanodes have been made by chemical vapor deposition [97,103]. A versatile synthesis procedure, allowing performance optimization by doping, has been obtained by the hydrothermal route [104–107]. An equally versatile, room temperature procedure for hematite film formation and doping is realized by electrodeposition [98–100,102,108,109].

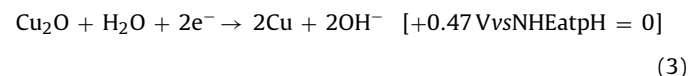
Hematite electrodeposition is simple and easy. However, the obtained photocurrents are relatively small [102]. As it happens in the case of BiVO<sub>4</sub>, one way to improve hematite photoanode performance is to introduce metal dopants (*i.e.* impurities) which improve electronic properties of the semiconductor photocatalyst. Metal impurities usually possess a valence of 2<sup>+</sup> or 4<sup>+</sup>, *i.e.* different form of that of Fe<sup>3+</sup>. Doping is expected to repair defects

and thus decrease electron-hole recombination. Metal doping thus involves a variety of dopants, for example, Pt [100], Zn and Ti [102,109]. Electrodeposition is usually followed by high temperature annealing, which affects grain size and grain boundaries and, subsequently, overall photocatalyst performance [110]. In addition, it leads to unintentional doping with Sn deriving from the FTO (Fluorine doped Tin Oxide) substrate, which is usually employed as transparent electrode [107]. This unintentional doping also contributes to modification of hematite photoanode performance so that annealing temperature becomes important also for this reason. The effect of metal doping on the photocurrent can be, for example, seen in Ref. [102] where the photocurrent more than doubled by introduction of Ti<sup>4+</sup> impurities.

Improvement of hematite photoanode performance can be also obtained by adding oxygen evolution catalysts [99], as in the case of WO<sub>3</sub> and BiVO<sub>4</sub>. However, this can be also obtained in the presence of an organic sacrificial agent [102], namely ethanol. Unfortunately, study of organic material photoelectrocatalytic degradation with hematite photoanodes is also soundly neglected. As in the case of BiVO<sub>4</sub>, it is obvious that this subject remains an unexplored but interesting research target.

## 4. Semiconductors for photocathodes

The choice of p-type photocatalysts is much more limited than n-type photocatalysts. The most important reason is that p-type semiconductors are very unstable in contact with an electrolyte. Therefore, they must be protected without losing their functionality and this is not easy. One of the most popular p-type photocatalysts is Cu<sub>2</sub>O, which is easy to synthesize, for example, by electrodeposition [22]. Its energy levels lie at –0.7 and 1.3 V vs SHE, for the CB and VB, respectively (*cf.* subsection 2.3 and Fig. 4). With an energy gap of 2.0 eV, its maximum expected photocurrent density is 14.7 mA cm<sup>-2</sup> and the solar to hydrogen efficiency (STH) 18% for irradiation equal to 1 sun [22]. Its CB is well placed for water reduction but for water oxidation an appropriate bias is necessary. Cu<sub>2</sub>O undergoes a reductive decomposition by the following reaction [22]:



Obviously, self-photoreduction of Cu<sub>2</sub>O is possible in the same way that self-photooxidation is possible for some n-type semiconductors. Several approaches have been adopted to provide protection for Cu<sub>2</sub>O. Thus by depositing a thin layer of titania and ZnO by atomic layer deposition (ALD) the photocurrent was tripled and the lifetime of the photocathode became substantially longer [22]. Other protective layers, which were presented in recent publications, include SnO<sub>2</sub> [111], Ga<sub>2</sub>O<sub>3</sub> [112], carbon [113], Cu<sub>2</sub>S [114], etc.

The role of the photocathode is to exchange electrons with the electrolyte. This exchange is obstructed by the overpotential that develops between the two phases. For this reason and in order to overcome overpotential, in addition to the protective layer, a co-catalyst is also necessary. Pt has been, of course, used as co-catalyst [112], as well as RuO<sub>2</sub> [111] and NiOx [115].

Another category of p-type photocatalysts, copper based chalcogenide semiconductors, have also been widely used as photocathodes [116]. Cu(In,Ga)Se<sub>2</sub> (CIGS) and Cu<sub>2</sub>ZnSnS<sub>4</sub> (CZTS), the most characteristic semiconductors of that family, have been successfully used in photovoltaics but they are also successfully employed as photocathodes for WS applications. Ref. [116] presents a review of this family of materials. CIGS photocathodes provide the possibility of tuning band gap in the range between 1.0–1.7 eV by

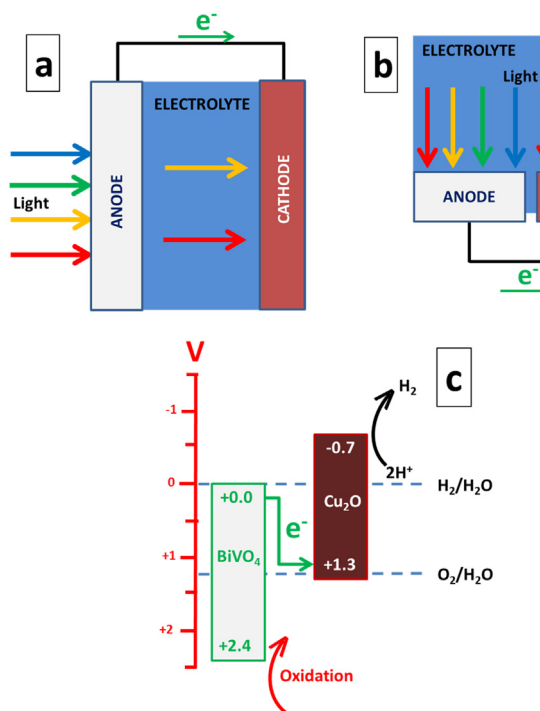


**Fig. 11.** Schematic illustration of a combined photoanode-photocathode tandem cell: (a) tandem configuration; (b) parallel illumination and (c) energy diagram (cf. Refs. [145,146]).

modifying composition [116]. Another advantage is that they have a large absorption coefficient of the order of  $10^5 \text{ cm}^{-1}$  [117]. The position of the CB is around  $-1.0 \text{ V}$  vs NHE [118] but CIGS has a very shallow VB (much less than  $+1.23 \text{ V}$  vs NHE), therefore it necessitates a strong bias to run the cell (cf. Fig. 4 and Fig. 9). As it happens with all p-type materials, it necessitates a protective over layer and addition of hydrogen evolution catalysts (HEC) to deal with strong overpotential between electrode and electrolyte. In a characteristic example given in [118], two n-type semiconductor layers and a Pt co-catalyst were necessary in order to provide protection and create a cascade electron transfer (cf. Fig. 9). This design was rewarding because it provided high current flow [118].

CIGS and other chalcopyrite semiconductors contain In and Ga which are rare and expensive. For this reason, research has turned to  $\text{Cu}_2\text{ZnSnS}_4$  (CZTS)-type copper chalcogenides (kesterite photocathodes), composed of more abundant materials, also not containing toxic Se [116,119]. A review of CZTS photocathodes is given in [119]. In general, research on CZTS follows the same trends as for CIGS. Thus increase of PEC performance by using CZTS photocathodes is gained by deposition of n-type semiconductor coverage plus noble metal co-catalyst [120]. A standard practice with both CIGS and CZTS photocathodes is also to use Mo instead of FTO electrodes [120]. In the above variants, cell performance was studied in a 3-electrode configuration where the current was observed under bias. However, in Ref. [120] an interesting combination between a CZTS photocathode and a  $\text{BiVO}_4$  photoanode was also presented, which run in a 2-electrode configuration without bias. In other words, it is possible to construct a WS device which runs without external bias by combining a photocathode with a photoanode electrode (see Tandem cells in Section 7.1).

## 5. Choice of counter electrodes

When a PEC cell operates with one photoactive electrode, the structure of the counter electrode is associated with the type of operation, i.e. whether it produces electricity or hydrogen. In the

first case, as already explained, oxygen is reduced, therefore the counter electrode must be in contact with air. It is then preferable to use an “air-breathing” electrode, which is usually made of carbon cloth or carbon paper on which the reduction electrocatalyst is deposited. In the case of hydrogen production, the electrode must operate in an inert environment, usually deoxygenated water, where the electrode is immersed. In most studies, a Pt sheet or Pt wire is used for this purpose. However, Pt is rare and expensive, therefore, it discourages massive application. For this reason, there is a strong effort for the search of alternative electrocatalysts. Fortunately, this domain is greatly supported by parallel studies on fuel cells and water electrolysis, where the search for alternative electrocatalysts is more crucial. Indeed, current limitations in PEC cells mainly arise from the constraints imposed by photocatalysts and photoelectrodes. Therefore, optimization of photocatalysts is a more crucial issue than optimization of electrocatalysts. Nevertheless, in the following paragraphs a short account is made on characteristic types of counter electrodes and electrocatalysts.

### 5.1. Oxygen reduction electrocatalysts

Electrocatalysts should possess three basic properties: electric conductivity, high SSA and active sites. Experience with fuel cells shows that a mixture of nanoparticulate Pt with carbon nanoparticles (Pt/C), for example carbon black, makes a very good electrocatalyst. By depositing this mixture on a carbon cloth (CC) by using appropriate hydrophobic pastes, one can make an efficient air-breathing counter electrode appropriate for oxygen reduction. Indeed, such electrodes have been used both for fuel cells and PFCs [17,41,121–126]. However, Pt is rare and expensive. In addition, Pt nanoparticles have the tendency to aggregate and this leads to progressive decrease of their electrocatalytic efficiency. It is then necessary to search for alternative oxygen reduction electrocatalysts. There are some studies on this matter, which were designed for PFCs. For example, in [127] a bucky paper (i.e. made of carbon nanotubes) was used as counter electrode, in [128] a CC was functionalized with polypyrrole and in [129] a high SSA material was employed, which was made of sulfur-doped porous carbon nanosheets [130,131]. Alternative oxygen reduction electrocatalysts have mainly been studied for fuel cells. There are literally thousands of papers published for this purpose. Some recent reviews can be found in Refs. [132–135]. All this great experience can be exploited for constructing efficient Pt-free PFCs. This matter has not been sufficiently dealt with because, as already said, in photoelectrocatalysis the focus is placed on photocatalysts. Thus this matter opens large research possibilities.

### 5.2. Hydrogen evolution electrocatalysts

When the cell functions for hydrogen production operation, the counter electrode carries a hydrogen evolution electrocatalyst. Most researchers utilize for this purpose a Pt foil, a Pt wire or a standard Pt/C electrocatalyst deposited on an electrode [26,61,82,84,102,136]. Recent works focus on optimization of photocathodes along the general lines analyzed in Section 4. As it happens with oxygen evolution electrocatalysts, there is a lot of work being carried out for developing Pt-free electrocatalysts for fuel cells and water electrolysis. Some reviews can be found in Refs. [137–139]. Photoelectrocatalytic WS should benefit from this rich knowhow, as suggested for oxygen reduction electrocatalysts.

In the case of sulfur-containing electrolytes, Pt/C electrocatalysts are useless since they are neutralized by chemical interactions. In that case, it is preferable to use nanostructured metal sulfides as electrocatalysts [11,43,140,141]. These structures can be easily made by simple procedures. For example,  $\text{CuS}$  and  $\text{CoS}$  can be deposited by electrodeposition [142] while  $\text{Cu}_2\text{S}$  can be formed on

a brass foil by simple chemical corrosion [11]. Fig. 10 gives SEM images of these two electrocatalysts.

## 6. Choice of electrolytes

The choice of electrolytes for both PFC and WS operation of photoelectrocatalytic cells is rather limited. This allows researchers to limit the parameters involved and have a better comparison between the published results. The choice is dictated by the nature of the photocatalyst and the pH of the solution. Chalcogenide semiconductor photoanodes or sensitized photoanodes have been frequently used in the presence of combined sulfide-sulfite electrolyte [11,143], which is used both as electrolyte and inorganic sacrificial agent (*cf.* Table 2, Reactions (2.1) and (2.2)). If the sacrificial-agent property is not necessary, for example in the case of photocathodes, stable sulfate electrolytes have been used instead of the sulfide-sulfite combination [114,118]. Mostly alkaline electrolyte is used with titania or hematite photoanodes [17,41,97,102,144], however,  $\text{WO}_3$  is stable only in acidic environment and necessitates neutral or acidic electrolytes [61,70,71]. Likewise for  $\text{BiVO}_4$  photoanodes which have been employed in the presence of  $\text{NaHCO}_3$  [84],  $\text{Na}_2\text{SO}_4$  [85], etc.

## 7. Selected topics related with PFC and WS operation

### 7.1. Tandem cells for photoelectrocatalytic operation

In the previous sections, discussion has been carried upon simple photoelectrocatalysis cells which consist of a photoactive electrode (photoanode or photocathode) and a counter electrode. Such a cell necessitates application of an external bias in order to produce hydrogen by water splitting. It is obvious that unassisted cells, which may produce hydrogen only by insolation without application of an external bias, are of great interest. There are three types of unassisted cells [145]: photoelectrolysis devices where the electric energy needed for electrolysis derives from renewable electricity, for example, a photovoltaic (PV) cell; a tandem cell made by a combination of a photocathode with a photoanode; and a tandem cell combined with a PV cell. In the present subsection, we will briefly describe tandem cells. More details can be found in the review paper of Ref. [145].

A simplified schematic diagram of a combined photoanode-photocathode tandem cell is given in Fig. 11. The two photoactive electrodes may be placed in a tandem (series) configuration as in Fig. 11a. This configuration applies to a photoanode with a larger band gap than that of the photocathode. Thus the photoanode absorbs mainly the shorter wavelength radiation while the rest is absorbed by the photocathode. In this way, the system may absorb light in the whole spectrum of the visible light and thus produce high current and attain large STH efficiency. The electrodes may also be placed side by side, as in Fig. 11b and be activated by parallel illumination. In that case, the whole solar spectrum is available to both electrodes and the photoanode is not necessary to be transparent, however, the distance between the two electrodes is larger, therefore the internal resistance of the cell is in that case also larger. On the contrary, in a tandem configuration the electrodes can be brought very close to each other. The designs of Fig. 11 are not exclusive. Other designs may be also proposed. Fig. 11c gives an example of a tandem cell, *i.e.* a combination between a  $\text{BiVO}_4$  photoanode and a  $\text{Cu}_2\text{O}$  photocathode [146]. Another combination, this time between a CZTS photocathode and  $\text{BiVO}_4$  photoanode is given in [120]. Fig. 11c explains the functionality of combined photoanode-photocathode tandem cells. Photons are absorbed by both electrodes. Photogenerated holes in the VB of the photoanode are consumed by oxidation reactions. Photogenerated electrons in

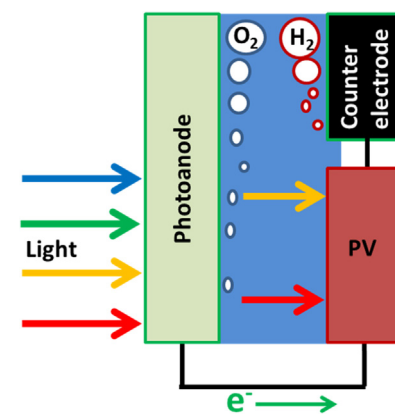


**Fig. 12.** Schematic illustration of a tandem combination of a WS device with a PV cell.

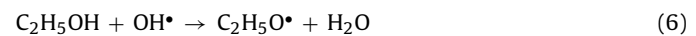
the CB of the photocathode are consumed by reduction reactions. An ohmic contact between photoanode and photocathode allows photogenerated electrons in the CB of the photoanode to compensate holes left in the VB of the photocathode.

In the case of the second tandem cell type, a combination is made between a photoelectrochemical cell and a PV cell [145]. Even though, classical PV cells may be used for this purpose, many researchers prefer to combine recently developed sensitized solar cells with WS devices [20,145,147–149]. A simplified illustration of a tandem cell of this category is shown in Fig. 12. In other words, the bias necessary for running the WS device is provided by the PV cell positioned in a tandem configuration.

Tandem cells have been exclusively designed for WS applications. They could also be used in the presence of sacrificial organic or inorganic agents and they are expected to lead to unassisted hydrogen production by oxidation of the sacrificial agents. This is a rather virgin field, which is worth studying.

### 7.2. Current doubling

Current doubling is a phenomenon observed during photoelectrocatalytic oxidation of sacrificial agents. In the presence of an organic fuel or an inorganic sacrificial agent, photogenerated holes are more effectively scavenged than in their absence. This leads to an increase of the current flowing through the cell. However, this increase sometimes is so high that the number of electrons flowing through the cell is larger than the number of photons absorbed [150]. This impressive phenomenon is explained by the creation of unstable radicals by oxidation of the fuel and the subsequent injection of electrons into the CB of the photocatalyst [53,62–65]. For example, in the case of ethanol the following oxidation reactions may take place:



Reaction (4) is a two-hole oxidation of ethanol to acetaldehyde, however, Reactions (5) and (6) are one-hole oxidations, either directly or by the intermediate of hydroxyl radicals, which create unstable  $\text{C}_2\text{H}_5\text{O}^\bullet$  radicals. These radicals can inject an electron into the CB of the photocatalyst. Thus it is possible for one photon absorbed to produce two electrons, one photogenerated and one injected, hence current doubling. Current doubling is nicely demonstrated when the current of the cell is monitored under bias, as in the case of Fig. 8, where the current in the presence of ethanol was twice as large as in its absence. Current doubling phenomena may

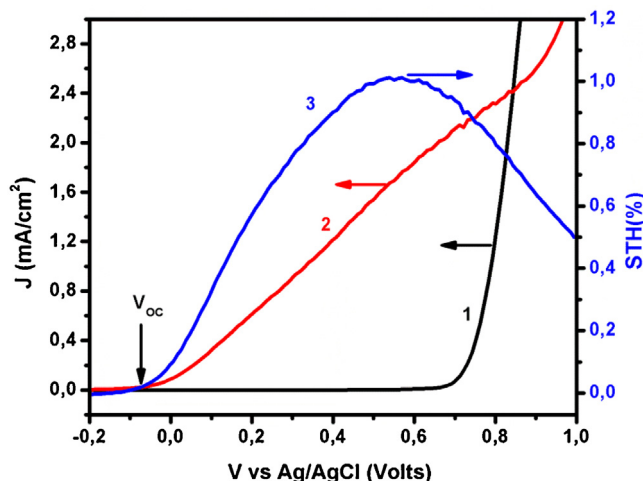
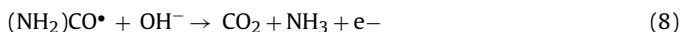
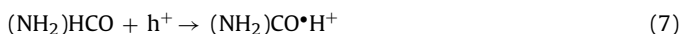


**Fig. 13.** Current-voltage curve for a Ti-modified  $\text{Fe}_2\text{O}_3$  photoanode (cf. Ref. [102]) in the dark (1) and under illumination (2). Curve (3) gives the corresponding STH values calculated according to equation (11) by using  $V_{\text{oc}} = -0.07 \text{ V}$  vs  $\text{Ag}/\text{AgCl}$ . Maximum STH efficiency was obtained at a bias of about  $0.55 \text{ V}$  vs  $\text{Ag}/\text{AgCl}$ .

be observed also in the presence of inorganic sacrificial agents, as for example in Ref. [13]. Thus in the case of formamide [13,151], the following charge injection may be envisaged



Current doubling phenomena are more clearly demonstrated under electric bias when electron-hole recombination is substantially limited.

### 7.3. Calculation of cell efficiency

Photoelectrocatalysis cells can be used either for electricity or solar fuel production. In both cases, the first thing that counts is to estimate the number of electrons produced as percentage of photons absorbed. This is nicely represented by the action spectrum, which is best expressed by IPCE (Incident Photon to Current Efficiency) values. IPCE is a measure of the effectiveness of the cell to convert the incident photons of a monochromatic radiation into electric current. It is given by the following equation [8,25]:

$$\text{IPCE} = \frac{1240 \times J_{\text{sc}}(\text{mA}/\text{cm}^2)}{\lambda(\text{nm}) \times P(\text{mW}/\text{cm}^2)} \quad (9)$$

where  $J_{\text{sc}}$  is the short-circuit current density and  $P$  the incident radiation intensity at a given wavelength  $\lambda$ . IPCE is a pure number without units. The number 1240 carries the matching units. By recording IPCE at different wavelengths, it is possible to judge the effectiveness of the cell with respect to the spectral response of a photocatalyst or a system of combined photocatalysts or a sensitized catalyst. The value of IPCE is expected to vary between 0 and 1 but researchers usually employ IPCE% values [152–154] obtained by simply multiplying IPCE by 100.

An unassisted cell producing electricity [17,122,155,156] can be characterized in the same manner as PV cells, i.e. by measuring its photovoltaic parameters: short circuit current density,  $J_{\text{sc}}$ , open circuit voltage,  $V_{\text{oc}}$  and fill factor, FF. The efficiency is then given by

$$\eta = \frac{J(\text{mA cm}^{-2}) \times V(\text{Volts}) \times FF}{P(\text{mW cm}^{-2})} \times 100 \text{ and } FF = \frac{(JV)_{\text{max}}}{J_{\text{sc}}V_{\text{oc}}} \quad (10)$$

where  $P$  represents the total incident light intensity and  $(JV)_{\text{max}}$  is the maximum electric power generated by the cell. It must be understood that in photoelectrocatalytic (photosynthetic) non

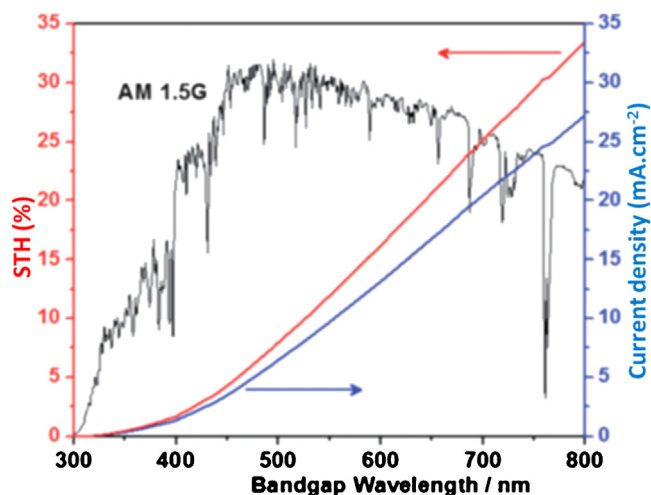


**Fig. 14.** Diagram showing the distribution of solar radiation and the variation of STH and maximum current density expectancy vs the absorption range of the photoactive electrode(s). (Based on a diagram in Ref. [80]).

regenerative cells, in addition to solar energy the chemical energy of the fuel is also consumed. However, the fuel is usually a waste. For this reason and for practical purposes, the formula of equation (10) may be employed.

For hydrogen production operation, solar to hydrogen (STH) efficiency is estimated by the standard formula [80,157]

$$\eta_{\text{STH}} = \frac{J(\text{mA cm}^{-2}) \times (1.23 - V_{\text{app}})(V)}{P(\text{mW cm}^{-2})} \times 100 \quad (11)$$

where  $V_{\text{app}}$  is given by the  $V_{\text{app}} = V_{\text{bias}} - V_{\text{oc}}$ .  $V_{\text{oc}}$  is the open circuit potential measured under the same conditions as the bias potential [158,159]. To make things clearer, Fig. 13 presents an example showing photocurrent and the corresponding calculated  $\eta_{\text{STH}}$  curve. Calculation of the efficiency is much simpler in the case of unassisted hydrogen production, as it happens with tandem cells where  $V_{\text{app}}$  is, of course, equal to zero [80,160]. The maximum current expected for each cell depends on the light absorption range, that is, on the band gap of the photocatalyst, in combination with the solar radiation for the corresponding wavelength range. This has been calculated in several occasions [150,161] and there are published lists and diagrams [20,21,80] which give the expected maximum current for every photocatalyst or combinations of photocatalysts. One such diagram selected from Ref [80], is reproduced in Fig. 14. For example, in the case of titania photoanodes sensitized by CdS-QDs, the combined band gap is about 2.5 eV ( $\sim 500 \text{ nm}$ ) and the maximum expected photocurrent density is approximately  $6.5 \text{ mA cm}^{-2}$  while for a CdSe/CdS/TiO<sub>2</sub> with absorbance up to  $650 \text{ nm}$ , i.e. a band gap  $< 2.0 \text{ eV}$ , the expected current density should be more than  $15 \text{ mA cm}^{-2}$ .

Solar to hydrogen  $\eta_{\text{STH}}$  efficiency, in reality, is the efficiency of the device and relates to its capacity to produce current. Flow of current does not guarantee that hydrogen will actually be produced. Therefore, calculation of  $\eta_{\text{STH}}$  should be accompanied by calculation of the faradaic efficiency, that is, the percentage of current which is converted into hydrogen. For this purpose, the following relation may be employed.

$$1 \mu\text{mol}/\text{min} \rightarrow \frac{10^{-6} \times 6.022 \times 10^{23} \times 2 \times 1.6 \times 10^{-19} \text{ C}}{60 \text{ s}} = 3.21 \text{ mA} \quad (12)$$

In this relation, we take into account that two electrons are necessary to form one hydrogen molecule. Therefore, 100% faradaic efficiency means that if the current flowing in the cell is 3.21 mA the hydrogen production rate should be  $1 \mu\text{mol}/\text{min}$ .

**Table 4**

Collection of recent data on PFC operation.

Sacrificial agent	Photocatalyst	Electro lyte	$J_{sc}$ ( $\text{mA cm}^{-2}$ )	$V_{oc}$ (V)	Maximum Power Density ( $\text{mW cm}^{-2}$ )	Ref.
Ethanol	TiO <sub>2</sub>	NaOH	0.79	1.2		[17]
Ethanol	CdS/TiO <sub>2</sub>	NaOH	6.9	1.2		[41]
Glucose	BiVO <sub>4</sub> /TiO <sub>2</sub>	ZnO/CuO	Na <sub>2</sub> SO <sub>4</sub>		0.116	[92]
Tetra cycline	BiVO <sub>4</sub> /WO <sub>3</sub>		KH <sub>2</sub> PO <sub>4</sub>	0.26	0.78	[93]
Methanol	TiO <sub>2</sub>	KOH	0.66	1.2		[124]
Reactive Green 19	ZnO	water	0.0427		0.0102	[156]
Methylene Blue	ZnO	water			0.0032	[162]
Reactive Black 5	ZnO	Na <sub>2</sub> SO <sub>4</sub>	1.3	0.908	0.335	[163]
Reactive Black 5	ZnO	MgSO <sub>4</sub>	1.2	0.628	0.256	[163]
Reactive Black 5	ZnO	NaCl	1.05	0.523	0.245	[163]
Glucose	TNT	Na <sub>2</sub> SO <sub>4</sub>	0.15	0.70		[164]
Rhodamine B	Ag/AgCl/GO ZnIn <sub>2</sub> S <sub>4</sub>	Na <sub>2</sub> SO <sub>4</sub>	0.5			[165]
Triethanol amine	TNT	Na <sub>2</sub> SO <sub>4</sub>	0.37	1.3	0.09	[166]
Methanol	TNT	Na <sub>2</sub> SO <sub>4</sub>	0.20	0.96	0.03	[166]
Glucose	TNT	Na <sub>2</sub> SO <sub>4</sub>	0.17	1.07	0.04	[166]
Methanol	WO <sub>3</sub> nanotubes	Na <sub>2</sub> SO <sub>4</sub>	0.06	0.52	0.004	[166]
Methanol	Nb <sub>2</sub> O <sub>5</sub> nanotubes	Na <sub>2</sub> SO <sub>4</sub>	0.02	0.96	0.004	[166]
Methanol	CdS-ZnS/TiO <sub>2</sub>	KOH			4.08	[126]
Glucose	CdS-ZnS/TiO <sub>2</sub>	KOH			3.92	[126]
Organic polymer +metal ions	TiO <sub>2</sub>	KOH	0.23	0.63	0.084	[167]
Acid Orange 7	TiO <sub>2</sub>	NaCl	0.4	0.75		[168]
Rhodamine B	TNT	NaCl	0.25	0.45	0.032	[169]
Rhodamine B	WO <sub>3</sub> /TNT CuO/TNT	Na <sub>2</sub> SO <sub>4</sub>	0.05	0.18		[170]

**Table 5**

Collection of recent data on photoelectrocatalytic hydrogen production by oxidation of organic sacrificial agents.

Sacrificial agent	Photocatalyst	Electro lyte	Current density ( $\text{mA cm}^{-2}$ )	Bias (V vs Ag/AgCl)	H <sub>2</sub> evolution rate ( $\mu\text{mol/min}$ )	Ref.
Water	WO <sub>3</sub>	NaClO <sub>4</sub>	3.0	1.6	2.0	[61]
Ethanol	WO <sub>3</sub>	NaClO <sub>4</sub>	6.0	1.6	7.3	[61]
Water	WO <sub>3</sub>	H <sub>2</sub> SO <sub>4</sub>	0.8			[66]
Glucose	WO <sub>3</sub>	H <sub>2</sub> SO <sub>4</sub>	1.4			[66]
Water	Ti-Fe <sub>2</sub> O <sub>3</sub>	NaOH	2.2	0.7	1.2	[102]
Ethanol	Ti-Fe <sub>2</sub> O <sub>3</sub>	NaOH	3.2	0.7	2.0	[102]
Ar+H <sub>2</sub> O	TiO <sub>2</sub>	Nafion	0.015			[172]
Ar+H <sub>2</sub> O+ Methanol (gas phase)	TiO <sub>2</sub>	Nafion	0.300			[170]
Formic acid	TiO <sub>2</sub>	H <sub>2</sub> SO <sub>4</sub>	0.15		0.045	[173]
Glycerol	Cu-Ni/TiO <sub>2</sub>	KOH			1.58	[174]
Ascorbate+glucose	CdS	Na <sub>2</sub> SO <sub>4</sub>	0.167		0.71	[175]
Water	Pd/TNT	KOH	0.6			[176]
Glucose	Pd/TNT	KOH	1.1		0.47	[176]

The energy content of molecular hydrogen is 285.8 kJ/mol, therefore, 1  $\mu\text{mol-H}_2/\text{min}$  corresponds to  $(285.8 \times 10^3 \text{ J/mol}) \times (10^{-6} \text{ mol/60s}) = 4.76 \text{ mW}$ . For an incident solar radiation of  $100 \text{ mW cm}^{-2}$ , in terms of energy yield, 1  $\mu\text{mol-H}_2/\text{min}$  corresponds to 4.76% of renewable energy production (per  $\text{cm}^2$ ). In order then to achieve an efficiency of around 15%, which is equivalent to the energy produced by commercial PV panels, it is necessary to produce at least three times the above quantity or  $3 \times 1 \mu\text{mol-H}_2/\text{min}$  per  $\text{cm}^2$  of active electrode or a current density at least  $3 \times 3.21 = 9.63 \text{ mA cm}^{-2}$ . This current corresponds, of course, to a faradaic efficiency of 100%. If faradaic efficiency of the cell is less, the lower current limit will accordingly increase. Thus a CdSe/CdS/TiO<sub>2</sub> combined photoanode with maximum current density expectancy of  $15 \text{ mA cm}^{-2}$  is potentially capable of producing sufficient quantity of hydrogen for commercial applications.

## 8. Collection of data from recent publications

The present section contains data concerning all aspects of PFC and WS operation. The number of publications on water splitting is enormous but those which deal with PFC operation are lim-

ited. There is no obvious explanation of this difference. The idea of splitting water by using solar radiation is very attractive and it is based on the general frame of natural photosynthesis. However, production of renewable energy with simultaneous photocatalytic degradation of wastes or pollutants is also a very interesting project and deserves equivalent attention.

### 8.1. Electricity production by photocatalytic fuel cells (PFCs)

As analyzed in the previous sections, PFCs produce electricity by oxidizing an organic substance (fuel) at the photoanode and by reducing oxygen at the counter electrode. Table 4 summarizes data collected from recent papers concerning PFC operation [17,41,92,93,124,156,162–170].

The data of Table 4 were obtained with various light sources of various intensities and spectral range and they cannot be correctly compared, however, analysis of the content of the listed papers leads to the following conclusions. Titania is the standard photocatalytic material to make photoanodes for PFC operation while titania nanotubes (TNT), obtained by anodization of Ti, is a popular choice for a photoanode. Several dyes have been used as model pollutants in the sense that a PFC is designed to produce energy

**Table 6**

Collection of recent data on photoelectrocatalytic hydrogen production by oxidation of sulfide/sulfite sacrificial agents.

Photocatalyst	Current density (mA cm <sup>-2</sup> )	Photoanode active area (cm <sup>2</sup> )	H <sub>2</sub> evolution Rate		Faradaic Efficiency (%)	Ref.
			μmol/min	mL/h cm <sup>2</sup>		
CdSe/CdS/TiO <sub>2</sub>	7.0	12	3.7	0.41		[11]
ZnS/CdSe/CdS/TiO <sub>2</sub>	10.0	<0.40				[141]
ZnS/CdS/TiO <sub>2</sub>	3.3	<0.23		1.21		[177]
CdSe/TiO <sub>2</sub>	0.75			0.29		[178]
CdSe/TiO <sub>2</sub>	2.1	10	5.5	0.74		[179]
CdS/TiO <sub>2</sub> /CdSe	4.0	0.25				[180]
CdS/SnO <sub>2</sub>	9.9	~0.38		3.58	86	[181]
CdS/BaSnO <sub>3</sub>	4.8			1.61	80	[182]

by degrading pollutants and wastes. However, oxygenates of the general formula C<sub>x</sub>H<sub>y</sub>O<sub>z</sub> make the best fuel with the highest electric power yield. CdS sensitized titania produces, as expected, the highest currents, thanks to its visible light response. As discussed in Section 3.1, there are in fact only a few metal sulfide quantum dots which can be employed as sensitizers of titania, because the combined photocatalyst-sensitizer system must preserve its oxidative power [41]. Only a couple of metal sulfide sensitizers preserve this property, namely, CdS, ZnSe and some CdS-ZnS combinations [44,150,171]. ZnS alone is a large band gap semiconductor not absorbing in the Visible.

The open-circuit voltage was the highest in the case of nanoparticulate titania. This can be associated with the data presented in Figs. 2 and 3b. Since titania has the highest lying CB, its difference ΔV from the oxygen reduction level is the largest and this reflects on V<sub>oc</sub>. The choice of electrolyte varies a lot. Many authors prefer a rather neutral electrolyte like Na<sub>2</sub>SO<sub>4</sub>, however, alkaline media facilitate oxygen reduction Reaction (3.4). As a consequence, higher current densities have been obtained in alkaline media.

The visible light absorbing semiconductors discussed in Section 3 have different VB levels and thus their oxidative power varies from one photocatalyst to the other. Unfortunately, there is no work being done to test their applicability in PFCs. At least, WO<sub>3</sub> should offer a satisfactory performance. It is obvious that this remains an issue and creates, as already said, an interesting field of research.

## 8.2. Hydrogen production by photoelectrocatalytic oxidation of organic substances

Photoelectrocatalytic oxidation of organic sacrificial agents produces higher photocurrents than water oxidation and should lead to higher hydrogen production rates. Table 5 presents a collection of related data found in recent publications [61,66,102,172–176].

The related published works are very limited in number. However, they suffice to draw some solid conclusions. The current flowing in the cell and the quantity of hydrogen produced is much larger in the presence of an organic sacrificial agent than in water. This has been observed by using various photocatalysts, including nanoparticulate TiO<sub>2</sub>, titania nanotubes, WO<sub>3</sub>, Ti-Fe<sub>2</sub>O<sub>3</sub>, etc. Biomass derivatives, including alcohols, organic acids and, generally, oxygenates are the materials of choice for photoelectrocatalytic hydrogen production, since they offer higher hydrogen production rates. This is justified by the higher current densities and by the fact that hydrogen ions may be available by their photocatalytic reforming (cf. Reaction (1.1), Table 1). WO<sub>3</sub> and Ti-modified Fe<sub>2</sub>O<sub>3</sub> are very efficient photocatalysts, thanks to their substantial absorbance in the Visible. In this respect, WO<sub>3</sub> gave satisfactory performance despite its shorter visible-light-absorption range, thanks to its better optoelectronic properties compared to Fe<sub>2</sub>O<sub>3</sub>. In all

cases, hydrogen was produced under external bias or in a tandem array where a solar cell offered the necessary bias.

## 8.3. Photoelectrocatalytic hydrogen production in the presence of inorganic sacrificial agents

Hydrogen can be produced in the presence of inorganic agents, which are non-reversibly oxidized. A characteristic case is sulfide/sulfite salt mixtures. Their oxidation reactions have been presented in Table 2, i.e. Reactions (2.1) and (2.2). There is a fundamental difference between these agents and organic materials as well as with other inorganic agents such as ammonia (Table 2) and water itself. Thus their oxidation does not liberate any protons. Their role is only to scavenge holes while hydrogen is produced by water reduction. For this reason, pure water splitting by water oxidation is frequently confused with hydrogen production in the presence of sulfide/sulfite reagents. Table 6 gives a collection of data concerning hydrogen production in their presence [11,141,177–182].

The most popular choice of a photoanode for hydrogen production in the presence of sulfide/sulfite mixtures is mesoporous titania decorated with CdS and/or CdSe QDs. This is in agreement with the analysis been carried out in Section 3.1. The presence of sulfide salt repairs self-photooxidation of the QDs, while the oxidation potential of these salts matches the oxidation level of the combined photocatalyst (cf. Fig. 7 and Table 2). The presence of a top layer of ZnS further guarantees stability [141] as it has been repeatedly shown in studies of quantum dot sensitized solar cells [183]. Many researchers use photoanodes with very small active surface, because this leads to better statistics. However, upscaling will dramatically lower these statistics.

Nanostructured metal sulfides are used as electrocatalysts for hydrogen evolution in the presence of sulfide/sulfite electrolytes, as already said in Section 5.2 (cf. Fig. 10). Among them, Cu<sub>2</sub>S is a popular choice [11,141]. The active area of the counter electrode has not been given equivalent attention as that of the photoanode but it should affect current, hydrogen evolution rate and faradaic efficiency of the cell, therefore, more studies are necessary to deal with this issue. The maximum current density expected for a CdSe/CdS/TiO<sub>2</sub> photoanode, as already said, is larger than 15 mA cm<sup>-2</sup>. Since the recorded current densities are substantially smaller, as seen in Table 6, there is still room for improvement of both photoanode and reduction electrocatalyst.

## 8.4. Water splitting processes

The greatest mass of publications on photoelectrocatalytic processes deals with pure water splitting producing oxygen at the anode and hydrogen at the cathode electrode. This matter has been treated in a large number of review papers [20,21,43,80,184–186]. In the present subsection, we will be limited only to some

**Table 7**

Collection of recent data on photoelectrocatalytic water splitting.

System studied	Photocurrent	Bias (V)	Ref.
		vs Ag/AgCl	
RuO <sub>2</sub> /SnO <sub>2</sub> /Cu <sub>2</sub> O/Au	-4.5	0.0	[111]
Cu <sub>2</sub> O	-8.4	0.0	[112]
Pt/Ga <sub>2</sub> O <sub>3</sub> /Cu <sub>2</sub> O	-4.0	0.0	[112]
Pt/TiO <sub>2</sub> /Ga <sub>2</sub> O <sub>3</sub> /Cu <sub>2</sub> O	-6.4	0.0	[112]
Carbon-coated Cu <sub>2</sub> O	-2.7	0.0	[113]
Pt/ZnO/CdS/CIGS	-32.5	-0.7	[118]
Pt/In <sub>2</sub> O <sub>3</sub> /CdS/CZTS	-9.3	0.0	[120]
CuBi <sub>2</sub> O <sub>4</sub>	-0.5	0.4	[154]
Hybrid organic-inorganic	-3.0	0.0	[187]
Co <sub>3</sub> O <sub>4</sub> and Co <sub>3</sub> O <sub>4</sub> /Ag	-4.73	-0.4	[188]
Hybrid organic-inorganic	-3.0	-0.5	[189]
Cu-Fe <sub>2</sub> O <sub>3</sub>	-5.34	-0.6	[190]
NiFe/Cu <sub>2</sub> O	-3.5	-0.8	[191]
NiBi <sub>i</sub> /H-BiVO <sub>4</sub>	2.26	0.79	[192]
NiFeO <sub>x</sub> /Fe <sub>2</sub> O <sub>3</sub>	1.5	1.0	[193]
Fe <sub>x</sub> Ni <sub>1-x</sub> /Bi <sub>2</sub> MoO <sub>6</sub> /Si	~1	1.0	[194]
Ni/ZnO	~1.5	0.75	[195]
NiSe <sub>2</sub> /Si	5.8	1.23	[196]
Ti-FeOOH/Ti-Fe <sub>2</sub> O <sub>3</sub>	4.06	1.23	[197]
Ir/Fe <sub>2</sub> O <sub>3</sub>	~1	1.23	[198]
BiVO <sub>4</sub> -Cu <sub>2</sub> O Tandem cell (dual photoelectrode)	~1	–	[146]
BiVO <sub>4</sub> /WO <sub>3</sub> Tandem cell (combination with a DSSC)	8.5	–	[148]
IrO <sub>2</sub> -Cu <sub>2</sub> O Tandem cell (dual photoelectrode) combined with a PV cell	~2	–	[199]
Fe <sub>2</sub> O <sub>3</sub>	~32	1.5	[200]

of the most recent publications in order to highlight recent trends. Table 7 gives a summary of results collected from Refs. [111–120,146,148,154,187–200].

A great deal of recent research concerns the study of photocathodes and of their combination with hydrogen evolution co-catalysts [111–113,118,120,154,187–191]. As already said, most p-type semiconductors are unstable in contact with electrolytes and they must be covered with a protective layer. Such a layer is obtained, for example, by a stable n-type oxide semiconductor. In addition, the presence of an n-type semiconductor creates n-p junction with the underlying p-type photocatalyst. n-p junctions facilitate electron-hole separation and, in some cases, they have produced very high photocurrents [118]. Concerning hydrogen evolution agents, noble metal co-catalysts are very effective for this purpose and have offered high photocurrents. Concerning p-type photocatalysts themselves, Cu<sub>2</sub>O, CIGS and CZTS remain the most efficient and most popular materials for photocathodes but other cases have also been studied.

As far as photoanodes are concerned, many works deal with the visible light absorbing BiVO<sub>4</sub> and Fe<sub>2</sub>O<sub>3</sub>. Effort is made to compensate for their high electron-hole recombination rates by combining them with oxygen evolution catalysts [192–198]. Oxygen evolution research is very intriguing because oxidation of water is much more difficult than its reduction, since it necessitates the simultaneous transfer of 4 electrons (*cf.* Reactions (1.3a) and (1.3b) of Table 1), while for reduction of water only two electrons are necessary (*cf.* Reactions (3.1) and (3.2) of Table 3). Nickel and iron compounds are most of times used as OEC since they are easy to synthesize and deposit contrary to, for example, standard CoPi catalysts [197]. Nevertheless, certain works deal with innovative materials, which offer substantial photocurrents, as the NiSe<sub>2</sub>/Si photoanode of Ref. [196].

The study of tandem cells is also among the current trends [146,148,199] in WS research. The obtained photocurrents are affected by cell design. Highest photocurrents are expected in cases when a photoelectrocatalytic cell is combined with an electricity generating solar cell.

Finally, an interesting case is presented by the last reference [200]. In that work, a new idea is proposed by treating the behavior

of a hematite photoanode under insolation by concentrated light of intensity of several suns. The authors thus searched for optimal conditions of film thickness and materials stability.

## 9. Summary and perspectives

The present review has dealt with the most essential aspects of photoelectrocatalytic cells designed for either electricity or hydrogen production as important means of solar energy conversion. The function of a photoelectrocatalytic cell is based on the oxidation of an organic or an inorganic sacrificial agent, including water, and the reduction of water, protons or oxygen. Other reduction reactions, for example CO<sub>2</sub> reduction, have not been treated by the present review. Water splitting by oxidation, reduction or both as well as the oxidation of organic or inorganic wastes is the main target of photoelectrocatalytic cells. In the latter case, a double environmental benefit is gained by energy production and environmental remediation. All components of PEC cells have been reviewed, including photoanodes, photocathodes, counter electrodes and electrolytes. Several aspects of cell design have been examined including tandem cells and combination of electrodes. Materials used for the construction of all components have been reviewed and efficiency of the cells has been assessed. Finally, an account of very recent publications has been made revealing the recent trends in the study of this domain.

By running through the various sections of this paper, the following perspectives arise for the future. Photocatalytic fuel cells have been studied in a very limited number of works in spite of the fact that they offer higher energy yield than water splitting. They deserve higher attention. Most related works are limited to titania photoanodes and very few to visible light absorbing photocatalysts. There is an obvious need to make an assessment of the applicability of photocatalysts, such as WO<sub>3</sub>, BiVO<sub>4</sub> and Fe<sub>2</sub>O<sub>3</sub>, as photoanodes to photocatalytic fuel cells. The efficiency of the latter mainly depends on the functionality of the photoanodes and on their capacity to oxidize the fuel. The limitations imposed by the functionality or lack of functionality of the photoanodes resulted in a relative neglect of the study of counter electrodes and oxygen reduction electrocatalysts. However, photocatalytic fuel cell efficiency also depends on the

functionality of the counter electrode towards oxygen reduction. There exists a rich literature on the study of oxygen reduction electrocatalysts related with applications to fuel cells. Photocatalytic fuel cells may benefit from this knowledge, which can lead to the construction of Pt-free oxygen reduction electrocatalysts. The same reasoning is valid also for hydrogen and oxygen evolution electrocatalysts, which depend on Pt or other noble metals and necessitate the search for less expensive but equally functional materials. In this sense, an intriguing aspect of the functionality of counter electrodes is that most researchers are neglecting questions of size and active surface area, even though, for example, faradaic efficiency for hydrogen production should be associated with the properties of the counter electrode. This neglect derives from the limitations imposed by the photoelectrode, which may degrade the role of the counter electrode. In short, counter electrodes and electrocatalysts necessitate higher attention. Photoelectrocatalytic cells should benefit from the accumulated knowledge related with fuel cells and electrolyzers.

Photoelectrocatalytic cells constitute a relatively mature technology, despite the individual arising issues, as already explained. In this sense, it is necessary to work on cell design and confront upscaling problems, which have already been faced in regenerative solar cells. Tandem cells constitute a very nice design but in reality it remains a scientific curiosity without much consideration on design and materials cost. For example, a dual photoelectrode comprising both a photocathode and a photoanode may provide an unassisted cell operation but the costly materials employed may prove that a photoelectrocatalysis cell combined with a commercial PV cell is preferable in terms of construction cost.

## References

- [1] W.H. Brattain, C.G.B. Garrett, Experiments on the interface between germanium and an electrolyte, *Bell Syst. Tech. J.* 34 (1955) 129–176.
- [2] H. Gerischer, Electrochemical behavior of semiconductors under illumination, *J. Electrochem. Soc.* 113 (1966) 1174–1182.
- [3] M. Gratzel, Photoelectrochemical cells, *Nature* 414 (2001) 338–344.
- [4] E. Bequerel, Recherches sur les effets de la radiation chimique de la lumière solaire: au moyen des courants électriques, *C.R. Acad. Sci. 9* (1839) 145–149.
- [5] A. Fujishima, K. Honda, Electrochemical photolysis of water at a semiconductor electrode, *Nature* 238 (1972) 37–38.
- [6] B. O'Regan, M. Gratzel, A low-cost, high-efficiency solar cell based on dye-sensitized colloidal TiO<sub>2</sub> films, *Nature* 353 (1991) 737–740.
- [7] M. Kaneko, J. Nemoto, H. Ueno, N. Gokan, K. Ohnuki, M. Horikawa, R. Saito, T. Shibata, Photoelectrochemical reaction of biomass and bio-related compounds with nanoporous TiO<sub>2</sub> film photoanode and O<sub>2</sub>-reducing cathode, *Electrochim. Commun.* 8 (2006) 336–340.
- [8] P. Lianos, Production of electricity and hydrogen by photocatalytic degradation of organic wastes in a photoelectrochemical cell: the concept of the photofuelcell: a review of a Re-Emerging research field, *J. Hazard. Mater.* 185 (2011) 575–590.
- [9] R. Michal, S. Sfaelou, P. Lianos, Photocatalysis for renewable energy production using PhotoFuelCells, *Molecules* 19 (2014) 19732–19750.
- [10] S. Sfaelou, P. Lianos, Photoactivated Fuel Cells (PhotoFuelCells). An alternative source of renewable energy with environmental benefits, *AIMS Mater. Sci.* 3 (2016) 270–288.
- [11] M. Antoniadou, S. Sfaelou, V. Dracopoulos, P. Lianos, Platinum-free photoelectrochemical water splitting, *Catal. Commun.* 43 (2014) 72–74.
- [12] N. Buhler, K. Meier, J.F. Reber, Photochemical hydrogen production with cadmium sulfide suspensions, *J. Phys. Chem.* 88 (1984) 3261–3268.
- [13] L.-C. Pop, I. Tantis, P. Lianos, Photoelectrocatalytic hydrogen production using nitrogen containing water soluble wastes, *Int. J. Hydrogen Energy* 40 (2015) 8304–8310.
- [14] J. Nemoto, N. Gokan, H. Ueno, M. Kaneko, Photodecomposition of ammonia to dinitrogen and dihydrogen on platinized TiO<sub>2</sub> nanoparticles in an aqueous solution, *J. Photoch. Photobiol. A* 185 (2007) 295–300.
- [15] G.-L. Chiarello, M.H. Aguirre, E. Sell, Hydrogen production by photocatalytic steam reforming of methanol on noble metal-modified TiO<sub>2</sub>, *J. Catal.* 273 (2010) 182–190.
- [16] G.N. Nomikos, P. Panagiotopoulou, D.I. Kondarides, X. Verykios, Kinetic and mechanistic study of the photocatalytic reforming of methanol over Pt/TiO<sub>2</sub> catalyst, *Appl. Catal. B* 146 (2014) 249–257.
- [17] M. Antoniadou, P. Lianos, Production of electricity by photoelectrochemical oxidation of ethanol in a PhotoFuelCell, *Appl. Catal. B* 99 (2010) 307–313.
- [18] C.D. Jaeger, F.-R.F. Fan, A.J. Bard, Semiconductor electrodes. 26. Spectral sensitization of semiconductors with phthalocyanine, *J. Am. Chem. Soc.* 102 (1980) 2592–2597.
- [19] T. Nak, J. Nowotny, M. Rekas, C.C. Sorrell, Photo-electrochemical hydrogen generation from water using solar energy. Materials-related aspects, *Int. J. Hydrogen Energy* 27 (2002) 991–1022.
- [20] J. Li, N. Wu, Semiconductor-based photocatalysts and photoelectrochemical cells for solar fuel generation: a review, *Catal. Sci. Technol.* 5 (2015) 1360–1384.
- [21] Q. Huang, Z. Ye, X. Xiao, Recent progress in photocathodes for hydrogen evolution, *J. Mater. Chem. A* 3 (2015) 15824–15837.
- [22] A. Paracchino, V. Laporte, K. Sivula, M. Grätzel, E. Thimsen, Highly active oxide photocathode for photoelectrochemical water reduction, *Nat. Mater.* 10 (2011) 456–461.
- [23] N.K. Awad, E.A. Ashour, N.K. Allam, Recent advances in the use of metal oxide-based photocathodes for solar fuel production, *J. Renewable Sustainable Energy* 6 (2014), 022702-21p.
- [24] G.K. Mor, K. Shankar, M. Paulose, Enhanced photocleavage of water using titania nanotube arrays, *Nano Lett.* 5 (2005) 191–195.
- [25] O.K. Varghese, C.A. Grimes, Appropriate strategies for determining the photoconversion efficiency of water photoelectrolysis cells: a review with examples using titania nanotube array photoanodes, *Sol. Energy Mater. Sol. Cells* 92 (2008) 374–384.
- [26] T. Stoll, G. Zafeiropoulos, M.N. Tsampas, Solar fuel production in a novel polymeric electrolyte membrane photoelectrochemical (PEM-PEC) cell with a web of titania nanotube arrays as photoanode and gaseous reactants, *Int. J. Hydrogen Energy* 41 (2016) 17807–17817.
- [27] Y.X. Chen, A. Lavacchi, H.A. Miller, M. Bevilacqua, J. Filippi, M. Innocenti, A. Marchionni, W. Oberhauser, L. Wang, F. Vizza, Nanotechnology makes biomass electrolysis more energy efficient than water electrolysis, *Nat. Commun.* 5 (2014) 6, 4036.
- [28] L.G. Bettini, M.V. Dozzi, F. Della Foglia, G.L. Chiarello, E. Sell, C. Lenardi, P. Piseri, P. Milani, Mixed-phase nanocrystalline TiO<sub>2</sub> photocatalysts produced by flame spray pyrolysis, *Appl. Catal. B Environ.* 178 (2015) 226–232.
- [29] I. Tantis, M.V. Dozzi, L.G. Bettini, G.L. Chiarello, V. Dracopoulos, E. Sell, P. Lianos, High efficiency titania nanoparticles produced by flame spray pyrolysis. Photoelectrochemical and solar cell applications, *Appl. Catal. B* 182 (2016) 369–374.
- [30] M. Maisano, M.V. Dozzi, E. Sell, Searching for facet-dependent photoactivity of shape-controlled anatase TiO<sub>2</sub>, *J. Photochem. Photobiol. C* 28 (2016) 29–43.
- [31] X. Liu, F. Wang, Q. Wang, Nanostructure-based WO<sub>3</sub> photoanodes for photoelectrochemical water splitting, *Phys. Chem. Chem. Phys.* 14 (2012) 7894–7911.
- [32] E. Nouri, M.R. Mohammadi, Impact of preparation method of TiO<sub>2</sub>-RGO nanocomposite photoanodes on the performance of dye-sensitized solar cells, *Electrochim. Acta* 219 (2016) 38–48.
- [33] F. Ning, M. Shao, S. Xu, Y. Fu, R. Zhang, M. Wei, D.G. Evans, X. Duan, TiO<sub>2</sub>/graphene/NiFe-layered double hydroxide nanorod array photoanodes for efficient photoelectrochemical water splitting, *Energy Environ. Sci.* 9 (2016) 2633–2643.
- [34] X. Xu, B. Feng, G. Zhou, Z. Bao, J. Hu, Efficient photon harvesting and charge collection in 3D porous RGO-TiO<sub>2</sub> photoanode for solar water splitting, *Mater. Des.* 101 (2016) 95–101.
- [35] X. Li, G. Wang, L. Jing, W. Ni, H. Yan, C. Chen, Y. Yan, A photoelectrochemical methanol fuel cell based on aligned TiO<sub>2</sub> nanorods decorated graphene photoanode, *Chem. Commun.* 52 (2015) 2533–2536.
- [36] M.V. Dozzi, S. Marzorati, M. Longhi, M. Coduri, L. Artigliac, E. Sell, Photocatalytic activity of TiO<sub>2</sub>-WO<sub>3</sub> mixed oxides in relation to electron transfer efficiency, *Appl. Catal. B* 186 (2016) 157–165.
- [37] Y. Zhang, G. Zhao, H. Shi, Y. Zhang, W. Huang, X. Huang, Z. Wu, Photoelectrocatalytic glucose oxidation to promote hydrogen production over periodically ordered TiO<sub>2</sub> nanotube arrays assembled of Pd quantum dots, *Electrochim. Acta* 174 (2015) 93–101.
- [38] M. Antoniadou, P. Panagiotopoulou, D.I. Kondarides, P. Lianos, Photocatalysis and photoelectrocatalysis using nanocrystalline titania alone or combined with Pt, RuO<sub>2</sub> or NiO co-catalysts, *J. Appl. Electrochem.* 42 (2012) 737–743.
- [39] F. Xu, D. Bai, J. Mei, D. Wu, Z. Gao, K. Jiang, B. Liu, Enhanced photoelectrochemical performance with in-situ Au modified TiO<sub>2</sub> nanorod arrays as photoanode, *J. Alloys Compd* 688 (2016) 914–920.
- [40] Y.F. Nicolau, Solution deposition of thin solid compound films by a successive ionic-layer adsorption and reaction process, *Appl. Surf. Sci.* 22/23 (1985) 1061–1074.
- [41] S. Sfaelou, L. Sygelou, V. Dracopoulos, A. Travlos, P. Lianos, Effect of the nature of cadmium salts on the effectiveness of CdS SILAR deposition and its consequences on the performance of sensitized solar cells, *J. Phys. Chem. C* 118 (2014) 22873–22880.
- [42] R. Adhikari, L. Jin, F. Navarro-Pardo, D. Benetti, B. Al Otaibi, S. Vanka, H. Zhao, Z. Mi, A. Vomiero, F. Rosei, High efficiency, Pt-free photoelectrochemical cells for solar hydrogen generation based on giant quantum dots, *Nano Energy* 27 (2016) 265–274.
- [43] S. Sahai, A. Ikram, S. Rai, R. Shrivastav, S. Dass, V.R. Satsangi, Quantum dots sensitization for photoelectrochemical generation of hydrogen: a review, *Renewable Sustainabl Energy Rev.* 68 (2017) 19–27.

- [44] M. Antoniadou, S. Sfaelou, P. Lianos, Quantum dot sensitized titania for photo-fuel-cell and for water splitting operation in the presence of sacrificial agents, *Chem. Eng. J.* 254 (2014) 245–251.
- [45] P. Sudhagar, I. Herraiz-Cardona, H. Park, T. Song, S.H. Noh, S. Gimenez, I. Mora Sero, F. Fabregat-Santiago, J. Bisquert, C. Terashima, U. Paik, Y.S. Kang, A. Fujishima, T.H. Han, Exploring Graphene Quantum Dots/TiO<sub>2</sub> interface in photoelectrochemical reactions: solar to fuel conversion, *Electrochim. Acta* 187 (2016) 249–255.
- [46] H. Li, F. Li, Y. Wang, L. Bai, F. Yu, L. Sun, Visible-light-driven water oxidation on a photoanode by supramolecular assembly of photosensitizer and catalyst, *ChemPlusChem* 81 (2016) 1056–1059.
- [47] L.G. Devi, R. Kavitha, A review on non metal ion doped titania for the photocatalytic degradation of organic pollutants under UV/solar light: role of photogenerated charge carrier dynamics in enhancing the activity, *Appl. Catal. B* 140–141 (2013) 559–587.
- [48] C.-H. Lee, J.-L. Shie, Y.-T. Yang, C.-Y. Chang, Photoelectrochemical characteristics, photodegradation and kinetics of metal and non-metal elements co-doped photocatalyst for pollution removal, *Chem. Eng. J.* 303 (2016) 477–488.
- [49] E. Grabowska, Selected perovskite oxides: characterization, preparation and photocatalytic properties—a review, *Appl. Catal. B* 186 (2016) 97–126.
- [50] A. Kudo, Z-scheme photocatalyst systems for water splitting under visible light irradiation, *MRS Bull.* 36 (2011) 32–38.
- [51] G. Hodas, D. Cahen, J. Manassen, Tungsten trioxide as a photoanode for a photoelectrochemical cell (PEC), *Nature* 260 (1976) 312–313.
- [52] M. Ashokkumar, P. Maruthamuthu, Photocatalytic hydrogen production with semiconductor particulate systems: an effort to enhance the efficiency, *Int. J. Hydrogen Energy* 16 (9) (1991) 591–595.
- [53] B.D. Alexander, P.J. Kulesza, I. Rutkowska, R. Solarska, J. Augustynski, Metal oxide photoanodes for solar hydrogen production, *J. Mater. Chem.* 18 (2008) 2298–2303.
- [54] J. Gan, X. Lu, Y. Tong, Towards highly efficient photoanodes: boosting sunlight-Driven semiconductor nanomaterials for water oxidation, *Nanoscale* 6 (2014) 7142–7164.
- [55] T. Zhu, M.N. Chong, E.S. Chan, Nanostructured tungsten trioxide thin films synthesized for photoelectrocatalytic water oxidation: a review, *Chem. Sus. Chem.* 7 (2014) 2974–2997.
- [56] C. Janáky, K. Rajeshwar, N.R. de Tacconi, W. Chammanee, M.N. Huda, Tungsten-Based oxide semiconductors for solar hydrogen generation, *Catal. Today* 199 (2013) 53–64.
- [57] C.C.L. McCrory, S. Jung, I.M. Ferrer, S. Chatman, J.C. Peters, T.F. Jarillo-Herrero, Benchmarking, OER electrocatalysts for solar water splitting devices, *J. Am. Chem. Soc.* 137 (2015) 4347–4357.
- [58] M. Sarnowska, K. Bienkowski, P.J. Barczuk, R. Solarska, J. Augustynski, Highly efficient and stable solar water splitting at (Na)WO<sub>3</sub> photoanodes in acidic electrolyte assisted by non-noble metal oxygen evolution catalyst, *Adv. Energy Mater.* (2016) 1600526.
- [59] C. Fabrega, S. Murcia-Lopez, D. Monllor-Satoca, J.D. Prades, M.D. Hernandez-Alonso, G. Penelas, J.R. Morante, T. Andreu, Efficient WO<sub>3</sub> photoanodes fabricated by pulsed laser deposition for photoelectrochemical water splitting with high faradaic efficiency, *Appl. Catal. B* 189 (2016) 133–140.
- [60] Y. Liu, J. Li, W. Li, H. He, Y. Yang, Y. Li, Q. Chen, Electrochemical doping induced In situ homo-species for enhanced photoelectrochemical performance on WO<sub>3</sub> nanoparticles film photoelectrodes, *Electrochim. Acta* 210 (2016) 251–260.
- [61] S. Sfaelou, L.-C. Pop, O. Monfort, V. Dracopoulos, P. Lianos, Mesoporous WO<sub>3</sub> photoanodes for hydrogen production by water splitting and PhotoFuelCell operation, *Int. J. Hydrogen Energy* 41 (2016) 5902–5907.
- [62] S.R. Morisson, T. Freund, Chemical role of holes and electrons in ZnO photocatalysis, *J. Chem. Phys.* 47 (1967) 1543–1551.
- [63] Y. Maeda, A. Fujishima, K. Honda, The investigation of current doubling reactions on semiconductor photoelectrodes by temperature change measurements, *J. Electrochem. Soc.* 178 (1981) 1731–1734.
- [64] T. Ohno, S. Izumi, K. Fujihara, Y. Masaki, M. Matsumura, Vanishing of current-doubling effect in photooxidation of 2-propanol on TiO<sub>2</sub> in solutions containing Fe(III) ions, *J. Phys. Chem. B* 104 (2000) 6801–6803.
- [65] E. Kalamaras, P. Lianos, Current doubling effect revisited: current multiplication in a PhotoFuelCell, *J. Electroanal. Chem.* 751 (2015) 37–42.
- [66] D.V. Esposito, R.V. Forest, Y. Chang, N. Gaillard, B.E. McCandless, S. Hou, K.H. Lee, R.W. Birkmire, J.G. Chen, Photoelectrochemical reforming of glucose for hydrogen production using a WO<sub>3</sub>-based tandem cell device, *Energy Environ. Sci.* 5 (2012) 9091–9099.
- [67] T. Lee, Y. Lee, W. Jang, A. Soon, Understanding the advantage of hexagonal WO<sub>3</sub> as an efficient photoanode for solar water splitting: a first-principles perspective, *J. Mater. Chem. A* 4 (2016) 11498–11506.
- [68] Q. Zeng, J. Li, J. Bai, X. Li, L. Xia, B. Zhou, Preparation of vertically aligned WO nanoplate array films based on peroxotungstate reduction reaction and their excellent photoelectrocatalytic performance, *Appl. Catal. B* 202 (2017) 388–396.
- [69] J. Zhang, H. Ma, Z. Liu, Highly efficient photocatalyst based on all oxides WO<sub>3</sub>/Cu<sub>2</sub>O heterojunction for photoelectrochemical water splitting, *Appl. Catal. B* 201 (2017) 84–91.
- [70] Z. Liu, J. Wu, J. Zhang, Quantum dots and plasmonic Ag decorated WO<sub>3</sub> nanorod photoanodes with enhanced photoelectrochemical performances, *Int. J. Hydrogen Energy* 41 (2016) 20529–20535.
- [71] S. Reinhard, F. Rechberger, M. Niederberger, Commercially available WO<sub>3</sub> nanopowders for photoelectrochemical water splitting: photocurrent versus oxygen evolution, *ChemPlusChem* 81 (2016) 1–7.
- [72] L. Han, S. Dong, E. Wang, Transition-metal (Co,Ni, and Fe)-based electrocatalysts for the water oxidation reaction, *Adv. Mater.* 28 (2016) 9266–9291.
- [73] W.L. Kwong, C.C. Lee, J. Messinger, Transparent nanoparticulate FeOOH improves the performance of a WO<sub>3</sub> photoanode in a tandem water-splitting device, *J. Phys. Chem. C* 120 (2016) 10941–10950.
- [74] A. Kudo, K. Ueda, H. Kato, I. Mikami, Photocatalytic O<sub>2</sub> evolution under visible light irradiation on BiVO<sub>4</sub> in aqueous AgNO<sub>3</sub> solution, *Cat. Lett.* 53 (1998) 229–230.
- [75] K. Sayama, A. Nomura, Z. Zou, R. Abe, Y. Abe, H. Arakawa, Photoelectrochemical decomposition of water on Nanocrystalline BiVO<sub>4</sub> film electrodes under visible light, *Chem. Commun.* 290 (2003) 2908–2909.
- [76] Q. Jia, K. Iwashina, A. Kudo, Facile fabrication of an efficient BiVO<sub>4</sub> thin film electrode for water splitting under visible light irradiation, *PNAS* 109 (2012) 11564–11569.
- [77] Z. Huang, I. Pan, J. Zou, X. Zhang, L. Wang, Nanostructured bismuth vanadate-based materials for solar-energy-driven water oxidation: a review on recent progress, *Nanoscale* 6 (2014) 14044–14063.
- [78] P. Chatchai, Y. Murakami, S. Kishioka, A.Y. Nosaka, Y. Nosaka, Efficient photocatalytic activity of water oxidation over WO<sub>3</sub>/BiVO<sub>4</sub> composite under visible light irradiation, *Electrochim. Acta* 54 (2009) 1147–1152.
- [79] S. Moniz, S.A. Shevlin, D. Martin, Z. Guo, J. Tang, Visible-light driven heterojunction photocatalysts for water splitting—a critical review, *Energy Environ. Sci.* 8 (2015) 731–759.
- [80] Z. Li, W. Luo, M. Zhang, J. Feng, Z. Zou, Photoelectrochemical cells for solar hydrogen production: current state of promising photoelectrodes, methods to improve their properties, and outlook, *Energy Environ. Sci.* 6 (2013) 347–370.
- [81] S. Hernandez, G. Barbero, G. Saracco, A.-L. Alexe-Ionescu, Considerations on oxygen bubbles formation and evolution on BiVO<sub>4</sub> porous anodes used in water splitting photoelectrochemical cells, *J. Phys. Chem. C* 119 (18) (2015) 9916–9925.
- [82] O. Monfort, L.-C. Pop, S. Sfaelou, T. Plecenik, T. Roch, V. Dracopoulos, E. Stathatos, G. Plesch, P. Lianos, Photoelectrocatalytic hydrogen production by water splitting using BiVO<sub>4</sub> photoanodes, *Chem. Eng. J.* 286 (2016) 91–97.
- [83] H. Ye, J. Lee, J.S. Jang, A.J. Bard, Rapid screening of BiVO<sub>4</sub>-Based photocatalysts by scanning electrochemical microscopy (SECM) and studies of their photoelectrochemical properties, *J. Phys. Chem. C* 114 (2010) 13322–13328.
- [84] O. Monfort, S. Sfaelou, L. Satrapinskyy, T. Plecenik, T. Roch, G. Plesch, P. Lianos, Comparative study between pristine and Nb-modified BiVO<sub>4</sub> films employed for photoelectrocatalytic production of H<sub>2</sub> by water splitting and for photocatalytic degradation of organic pollutants under simulated solar light, *Catal. Today* 280 (2017) 51–57.
- [85] J. Quinonero, T. Lana-Villarreal, R. Gómez, Improving the photoactivity of bismuth vanadate thin film photoanodes through doping and surface modification strategies, *Appl. Catal. B* 194 (2016) 141–149.
- [86] R.P. Antony, P.S. Bassi, F.F. Abdi, S.Y. Chiam, Y. Ren, J. Barber, J.S.C. Loo, L.H. Wong, Electrosprayed Mo-BiVO<sub>4</sub> for efficient photoelectrochemical water oxidation: direct evidence of improved hole diffusion length and charge separation, *Electrochim. Acta* 211 (2016) 173–182.
- [87] Y. Zhang, Z. Yi, G. Wu, Q. Shen, Novel Y doped BiVO<sub>4</sub> thin film electrodes for enhanced photoelectric and photocatalytic performance, *J. Photoch. Photobiol. A* 327 (2016) 25–32.
- [88] A.J. Rettie, H.C. Lee, L.G. Marshall, J.F. Lin, C. Capan, J. Lindemuth, J.S. McCloy, J. Zhou, A.J. Bard, C.B. Mullins, Combined charge carrier transport and photoelectrochemical characterization of BiVO<sub>4</sub> single crystals: intrinsic behavior of a complex metal oxide, *J. Am. Chem. Soc.* 135 (2013) 11389–11396.
- [89] S.J.A. Moniz, J. Zhu, J. Tang, 1D Co-Pt modified BiVO<sub>4</sub>/ZnO junction cascade for efficient photoelectrochemical water cleavage, *Adv. Energy Mater.* 4 (2014) 1301590.
- [90] Y. Zhang, D. Wang, X. Zhang, Y. Chen, L. Kong, P. Chen, Y. Wang, C. Wang, L. Wang, Y. Liu, Enhanced photoelectrochemical performance of nanoporous BiVO<sub>4</sub> photoanode by combining surface deposited cobalt-phosphate with hydrogenation treatment, *Electrochim. Acta* 195 (2016) 51–58.
- [91] T.W. Kim, K.-S. Choi, Nanoporous BiVO<sub>4</sub> photoanodes with dual-layer oxygen evolution catalysts for solar water splitting, *Science* 343 (2014) 990–994.
- [92] J. Bai, R. Wang, Y. Li, Y. Tang, Q. Zeng, L. Xia, X. Li, J. Li, C. Li, B. Zhou, A solar light driven dual photoelectrode photocatalytic fuel cell (PFC) for simultaneous wastewater treatment and electricity generation, *J. Hazard. Mater.* 311 (2016) 51–62.
- [93] L. Xia, J. Bai, J. Li, Q. Zeng, X. Li, B. Zhou, A highly efficient BiVO<sub>4</sub>/WO<sub>3</sub>/W heterojunction photoanode for visible-light responsive dual photoelectrode photocatalytic fuel cell, *Appl. Catal. B* 183 (2016) 224–230.
- [94] K. Sivula, F. LeFormal, M. Grätzel, Solar water splitting: progress using hematite ( $\alpha$ -Fe<sub>2</sub>O<sub>3</sub>) photoelectrodes, *ChemSusChem* 4 (2011) 432–439.
- [95] Z. Shi, X. Wen, Z. Guan, D. Cao, W. Luo, Z. Zou, Recent progress in photoelectrochemical water splitting for solar hydrogen production, *Ann. Phys.* 358 (2014) 236–247.
- [96] M. Mishra, D.-M. Chun,  $\alpha$ -Fe<sub>2</sub>O<sub>3</sub> as a photocatalytic material: a review, *Appl. Catal. A* 498 (2015) 126–141.

- [97] S.C. Warren, K. Voitchkovsky, H. Dotan, C.M. Leroy, M. Cornuz, F. Stellacci, C. Hébert, A. Rothschild, M. Grätzel, Identifying champion nanostructures for solar water-splitting, *Nat. Mater.* 12 (2013) 842–849.
- [98] A. Bak, W. Choi, H. Park, Enhancing the photoelectrochemical performance of hematite ( $\alpha$ -Fe<sub>2</sub>O<sub>3</sub>) electrodes by cadmium incorporation, *Appl. Catal. B* 110 (2011) 207–215.
- [99] J.Y. Zheng, S.I. Son, T.K. Van, Y.S. Kang, Preparation of  $\alpha$ -Fe2O3 films by electrodeposition and photodeposition of Co-Pt on them to enhance their photoelectrochemical properties, *RSC Adv.* 5 (2015) 36307–36314.
- [100] G. Rahman, O.-S. Joo, Electrodeposited nanostructured  $\alpha$ -Fe2O3 thin films for solar water splitting: influence of Pt doping on photoelectrochemical performance, *Mater. Chem. Phys.* 140 (2013) 316–322.
- [101] M. Grätzel, Photoelectrochemical cells, *Nature* 414 (2001) 338–344.
- [102] E. Kalamaras, V. Dracopoulos, L. Sygellou, P. Lianos, Electrodeposited Ti-doped hematite photoanodes and their employment for photoelectrocatalytic hydrogen production in the presence of ethanol, *Chem. Eng. J.* 295 (2016) 288–294.
- [103] M. Cornuz, M. Grätzel, K. Sivula, Preferential orientation in hematite films for solar hydrogen production via water splitting, *Chem. Vap. Deposition* 16 (2010) 291–295.
- [104] L. Fu, H. Yu, C. Zhang, Z. Shao, B. Yi, Cobalt phosphate group modified hematite nanorod array as photoanode for efficient solar water splitting, *Electrochim. Acta* 136 (2014) 363–369.
- [105] Z. Fu, T. Jiang, Z. Liu, D. Wang, L. Wang, T. Xie, Highly photoactive Ti-doped  $\alpha$ -Fe2O3 nanorod arrays photoanode prepared by a hydrothermal method for photoelectrochemical water splitting, *Electrochim. Acta* 129 (2014) 358–363.
- [106] R. Rajendran, Z. Yaakob, M. Pudukudy, M.S.A. Rahaman, K. Sopian, Photoelectrochemical water splitting performance of vertically aligned hematite nanoflakes deposited on FTO by a hydrothermal method, *J. Alloys Compd.* 608 (2014) 207–212.
- [107] Y. Ling, Y. Li, Review of Sn-doped hematite nanostructures for photoelectrochemical water splitting, *Part. Part. Syst. Charact.* 31 (2014) 1113–1121.
- [108] R. Schreblé, K. Bello, F. Vera, P. Cury, E. Muñoz, R. Del Ro, H. Meier, R. Córdova, E. Dalchiele, An electrochemical deposition route for obtaining  $\alpha$ -Fe2O3 thin films, *Electrochim. Solid State Lett.* 9 (2006) C110–C113.
- [109] N. Mirbagheri, D. Wang, C. Peng, J. Wang, Q. Huang, C. Fan, E.E. Ferapontova, Visible light driven photoelectrochemical water oxidation by Zn- and Ti-doped hematite nanostructures, *ACS Catal.* 4 (2014) 2006–2015.
- [110] Y.W. Phuan, M.N. Chong, T. Zhu, S.-T. Yong, E.S. Chan, Effects of annealing temperature on the physicochemical, optical and photoelectrochemical properties of nanostructured hematite thin films prepared via electrodeposition method, *Mater. Res. Bull.* 69 (2015) 71–77.
- [111] J. Azevedo, S.D. Tilley, M. Schreier, M. Stefk, C. Sousa, J.P. Araújo, A. Mendes, M. Grätzel, M.T. Mayer, Tin oxide as stable protective layer for composite cuprous oxide water-splitting photocathodes, *Nano Energy* 24 (2016) 10–16.
- [112] C. Li, T. Hisatomi, O. Watanabe, M. Nakabayashi, N. Shibata, K. Domen, J.-J. Delaunay, Simultaneous enhancement of photovoltage and charge transfer in Cu2O-based photocathode using buffer and protective layers, *Appl. Phys. Lett.* 109 (2013) 033902.
- [113] W. Shi, X. Zhang, S. Li, B. Zhang, M. Wang, Y. She, Carbon coated Cu2O nanowires for photo-electrochemical water splitting with enhanced activity, *Appl. Surf. Sci.* 358 (2015) 404–411.
- [114] I. Minguez-Bacho, M. Courté, H.J. Fan, D. Fichou, Conformal Cu2S-coated Cu2O nanostructures grown by ion exchange reaction and their photoelectrochemical properties, *Nanotechnology* 26 (2015) 185401.
- [115] Y.-F. Lim, C.S. Chu, C.J.J. Lee, D. Chi, Sol-gel deposited Cu2O and CuO thin films for photocatalytic water splitting, *Phys. Chem. Chem. Phys.* 16 (2014) 25928–25934.
- [116] Y. Chen, X. Feng, M. Liu, J. Su, S. Shen, Towards efficient solar-to-hydrogen conversion: fundamentals and recent progress in copper-based chalcogenide photocathodes, *Nanophotonics* 5 (2016) 524–547.
- [117] S. Mandati, B.V. Sarada, S.R. Dey, S.V. Joshi, Photoelectrochemistry of Cu(In, Ga)Se<sub>2</sub> thin-films fabricated by sequential pulsed electrodeposition, *J. Power Sources* 273 (2015) 149–157.
- [118] M.G. Mali, H. Yoon, B. Joshi, H. Park, S.S. Al-Deyab, D.C. Lim, S. Ahn, C. Nervi, S.S. Yoon, Enhanced photoelectrochemical solar water splitting using a platinum-decorated CIGS/CdS/ZnO photocathode, *ACS Appl. Mater. Interfaces* 7 (2015) 21619–21625.
- [119] J. Wang, N. Yu, Y. Zhang, Y. Zhu, L. Fu, P. Zhang, L. Gao, Y. Wu, Synthesis and performance of Cu<sub>2</sub>ZnSnS<sub>4</sub> semiconductor as photocathode for solar water splitting, *J. Alloys Compd.* 688 (2016) 923–932.
- [120] F. Jiang, Gunawan, T. Harada, Y. Kuang, T. Minegishi, K. Domen, S. Ikeda, Pt/In<sub>2</sub>S<sub>3</sub>/CdS/Cu<sub>2</sub>ZnSnS<sub>4</sub> thin film as an efficient and stable photocathode for water reduction under sunlight radiation, *J. Am. Chem. Soc.* 137 (2015) 13691–13697.
- [121] Y.T. Law, S. Zafeiratos, S.G. Neophytides, A. Orfanidi, D. Costa, T. Dintzler, R. Arrigo, A. Knop-Gericke, R. Schlogl, E.R. Savinova, In situ investigation of dissociation and migration phenomena at the Pt/electrolyte interface of an electrochemical cell, *Chem. Sci.* 6 (2015) 5635–5642.
- [122] B. Wang, H. Zhang, X.-Y. Lu, J. Xuan, M.K.H. Leung, Solar photocatalytic fuel cell using CdS-TiO<sub>2</sub> photoanode and air-breathing cathode for wastewater treatment and simultaneous electricity production, *Chem. Eng. J.* 253 (2014) 174–182.
- [123] Q. Liao, L. Li, R. Chen, X. Zhu, H. Wang, D. Ye, X. Cheng, M. Zhang, Y. Zhou, Respective electrode potential characteristics of photocatalytic fuel cell with visible-light responsive photoanode and air-breathing cathode, *Int. J. Hydrogen Energy* 40 (2015) 16547–16555.
- [124] M. Xia, R. Chen, X. Zhu, Q. Liao, L. An, Z. Wang, X. He, L. Jiao, A micro photocatalytic fuel cell with an air-breathing, membraneless and monolithic design, *Sci. Bull.* 61 (2016) 1699–1710.
- [125] J. Rodriguez, E. Puzenata, P.-X. Thive, From solar photocatalysis to fuel-cell: a hydrogen supply chain, *J. Environ. Chem. Eng.* 4 (2016) 3001–3005.
- [126] L. Li, S. Xue, R. Chen, Q. Liao, X. Zhu, Z. Wang, X. He, H. Feng, X. Cheng, Performance characteristics of a membraneless solar responsive photocatalytic fuel cell with an air-breathing cathode under different fuels and electrolytes and air conditions, *Electrochim. Acta* 182 (2015) 280–288.
- [127] S. Sfaelou, M. Antoniadou, G. Trakakis, V. Dracopoulos, D. Tasis, J. Parthenios, C. Galiotis, K. Papagelis, P. Lianos, Buckypaper as Pt-free cathode electrode in photoactivated fuel cells, *Electrochim. Acta* 80 (2012) 399–404.
- [128] N. Balis, V. Dracopoulos, M. Antoniadou, P. Lianos, One-step electrodeposition of polypyrrole applied as oxygen reduction electrocatalyst in Photoactivated Fuel Cells, *Electrochim. Acta* 70 (2012) 338–343.
- [129] S. Sfaelou, X. Zhuang, X. Feng, P. Lianos, Sulfur-doped porous carbon nanosheets as high performance electrocatalysts for PhotoFuelCells, *RSC Adv.* 5 (2015) 27953–27963.
- [130] S. Li, D. Wu, H. Liang, J. Wang, X. Zhuang, Y. Mai, Y. Su, X. Feng, Metal-nitrogen doping of mesoporous carbon/graphene nanosheets by self-template for oxygen reduction electrocatalysts, *ChemSusChem* 7 (2014) 3002–3006.
- [131] Y. Su, Z. Yao, F. Zhang, H. Wang, Z. Mics, E. Cánovas, M. Bonn, X. Zhuang, X. Feng, Sulfur-enriched conjugated polymer nanosheet derived sulfur and nitrogen co-doped porous carbon nanosheets as electrocatalysts for oxygen reduction reaction and zinc-air battery, *Adv. Funct. Mater.* 26 (2016) 5893–5902.
- [132] Y. Lu, S. Du, R. Steinberger-Wilckens, One-dimensional nanostructured electrocatalysts for polymer electrolyte membrane fuel cells-a review, *Appl. Catal. B* 199 (2016) 292–314.
- [133] H. Erikson, A. Sarapuu, J. Solla-Gullón, K. Tammeveski, Recent progress in oxygen reduction electrocatalysis on Pd-based catalysts, *J. Electroanal. Chem.* 780 (2016) 327–336.
- [134] J. Coroa, M. Suárez, L.S.R. Silva, K.I.B. Eguiluz, G.R. Salazar-Banda, Fullerene applications in fuel cells: a review, *Int. J. Hydrogen Energy* 41 (2016) 17944–17959.
- [135] A. Brouzgou, S. Song, Z.-X. Liang, P. Tsiaikaras, Non-precious electrocatalysts for oxygen reduction reaction in alkaline media: latest achievements on novel carbon materials, *Catalysts* 6 (2016) 00159.
- [136] Y. Li, H. Yu, C. Zhang, W. Song, G. Li, Z. Shao, B. Yi, Effect of water and annealing temperature of anodized TiO<sub>2</sub> nanotubes on hydrogen production in photoelectrochemical cell, *Electrochim. Acta* 107 (2013) 313–319.
- [137] M.I. Jamesh, Recent progress on earth abundant hydrogen evolution reaction and oxygen evolution reaction bifunctional electrocatalyst for overall water splitting in alkaline media, *J. Power Sources* 333 (2016) 213–236.
- [138] M. Kuang, G. Zheng, Nanostructured bifunctional redox electrocatalysts, *Small* 12 (2016) 5656–5675.
- [139] W. Zhou, J. Jia, J. Lu, L. Yang, D. Hou, G. Li, S. Chen, Recent developments of carbon-based electrocatalysts for hydrogen evolution reaction, *Nano Energy* 28 (2016) 29–43.
- [140] J. Kibsgaard, T.F. Jaramillo, Molybdenum phosphosulfide: an active, acid-Stable, earth-Abundant catalyst for the hydrogen evolution reaction, *Angew. Chem.* 53 (2014) 14433–14437.
- [141] R. Adhikari, L. Jin, F. Navarro-Pardo, D. Benetti, B. AlOtaibi, S. Vanka, H. Zhao, Z. Mi, A. Vomiero, F. Rosei, High efficiency, Pt-free photoelectrochemical cells for solar hydrogen generation based on giant quantum dots, *Nano Energy* 27 (2016) 265–274.
- [142] N. Balis, V. Dracopoulos, K. Bourikas, P. Lianos, Quantum dot sensitized solar cells based on an optimized combination of ZnS, CdS and CdSe with CoS and CuS counter electrodes, *Electrochim. Acta* 91 (2013) 246–252.
- [143] C.-H. Chan, P. Samikkannu, H.-W. Wang, Fe<sub>2</sub>O<sub>3</sub>/CdS co-sensitized titania nanotube for hydrogen generation from photocatalytic splitting water, *Int. J. Hydrogen Energy* 41 (2016) 17818–17825.
- [144] M. Orlando, A. Mazzi, G. Arban, N. Bazzanella, P. Rudatis, S. Caramori, N. Patel, R. Fernandes, C.A. Bignozzi, A. Miotello, On the effect of Sn-doping in hematite anodes for oxygen evolution, *Electrochim. Acta* 214 (2016) 345–353.
- [145] K. Zhang, M. Ma, P. Li, D. Hwan Wang, H. Park, Water splitting progress in tandem devices: moving photolysis beyond electrolysis, *Adv. Energy Mater.* (2016) 1600602.
- [146] P. Bornoz, F.F. Abdi, S.D. Tilley, B. Dam, R. van de Krol, M. Graetzel, K. Sivula, A bismuth vanadate-cuprous oxide tandem cell for overall solar water splitting, *J. Phys. Chem. C* 118 (2014) 16959–16966.
- [147] J. Brillet, J.H. Yum, M. Cornuz, T. Hisatomi, R. Solarska, J. Augustynski, M. Graetzel, K. Sivula, Highly efficient water splitting by a dual-absorber tandem cell, *Nat. Photonics* 6 (2012) 824–828.
- [148] X. Shi, H. Jeong, S.J. Oh, M. Ma, K. Zhang, J. Kwon, I.T. Choi, I.Y. Choi, H.K. Kim, J.K. Kim, J.H. Park, Unassisted photoelectrochemical water splitting exceeding 7% solar-to-hydrogen conversion efficiency using photon recycling, *Nat. Commun.* 7 (2016) 11943.
- [149] S. Kosar, Y. Pihoshi, I. Turkevych, K. Mawatari, J. Uemura, Y. Kazoe, K. Makita, T. Sugaya, T. Matsui, D. Fujita, M. Tosa, Y.M. Struk, M. Kondo, T. Kitamori,

- Tandem photovoltaic-photoelectrochemical GaAs/InGaAsP-WO<sub>3</sub>/BiVO<sub>4</sub> device for solar hydrogen generation, *Japanese J. Appl. Phys.* 55 (2016) 04ES01.
- [150] M. Antoniadou, D.I. Kondarides, D.D. Dionysiou, P. Lianos, Quantum dot sensitized titania applicable as photoanode in photoactivated fuel cells, *J. Phys. Chem. C* 116 (2012) 16901–16909.
- [151] E. Pelizzetti, P. Calza, G. Mariella, V. Maurino, C. Minero, H. Hidaka, Different photocatalytic fate of amino nitrogen in formamide and urea, *Chem. Commun.* (2004) 1504–1505.
- [152] P.G. Ramos, N.J. Morales, R.J. Candal, M. Hojaberdiel, J. Rodriguez, Influence of zinc acetate content on the photoelectrochemical performance of zinc oxide nanostructures fabricated by electrospinning technique, *Nanometer. Nanotech.* 6 (2016) 1–7.
- [153] S. Emin, M. de Respinis, T. Mavrič, B. Damb, M. Valant, W.A. Smith, Photoelectrochemical water splitting with porous –Fe<sub>2</sub>O<sub>3</sub> thin films prepared from Fe/Fe-oxide nanoparticles, *Appl. Catal. A* 523 (2016) 130–138.
- [154] S.P. Berglund, F.F. Abdi, P. Bogdanoff, A. Chemseddine, D. Friedrich, R. van de Krol, Comprehensive evaluation of CuBi<sub>2</sub>O<sub>4</sub> as a photocathode material for photoelectrochemical water splitting, *Chem. Mater.* 28 (2016) 4231–4242.
- [155] T. Tang, K. Li, D. Ying, T. Sun, Y. Wang, J. Jia, High efficient aqueous-film rotating disk photocatalytic fuel cell (RDPFC) with triple functions: cogeneration of hydrogen and electricity with dye degradation, *Int. J. Hydrogen Energy* 39 (2014) 10258–10266.
- [156] S.-L. Lee, L.-N. Ho, S.-A. Ong, Y.-S. Wong, C.-H. Voon, W.F. Khalik, N.A. Yusoff, N. Nordin, A highly efficient immobilized ZnO/Zn photoanode for degradation of azo dye Reactive Green 19 in a photocatalytic fuel cell, *Chemosphere* 166 (2017) 118–125.
- [157] J.H. Kim, H. Kaneko, T. Minegishi, J. Kubota, K. Domen, J.S. Lee, Overall photoelectrochemical water splitting using tandem cell under simulated sunlight, *ChemSusChem* 9 (2016) 61–66.
- [158] S.U.M. Khan, M. Al-Shahry, W.B. Ingler Jr., Efficient photochemical water splitting by a chemically modified n-TiO<sub>x</sub>, *Science* 297 (2002) 2243–2245.
- [159] C.J. Lin, S.-J. Liao, L.-C. Kao, S.Y.H. Liou, Photoelectrocatalytic activity of a hydrothermally grown branched ZnO nanorod-array electrode for paracetamol degradation, *J. Hazard. Mater.* 291 (2015) 9–17.
- [160] A. Kargar, J. Khamwannah, C.-H. Liu, N. Park, D. Wang, S.A.S. Dayeh, Jin, Nanowire/nanotube array tandem cells for overall solar neutral water splitting, *Nano Energy* 19 (2016) 289–296.
- [161] A.B. Murphy, P.R.F. Barnes, L.K. Randeniya, I.C. Plumb, I.E. Grey, M.D. Horne, J.A. Glasscock, Efficiency of solar water splitting using semiconductor electrodes, *Int. J. Hydrogen Energy* 31 (2006) 1999–2017.
- [162] S.-L. Lee, L.-N. Ho, S.-A. Ong, G.-M. Lee, Y.-S. Wong, C.-H. Voon, W.F. Khalik, N.A. Yusoff, N. Nordin, Comparative study of photocatalytic fuel cell for degradation of methylene blue under sunlight and ultra-violet light irradiation, *Water Air Soil Pollut.* 227 (445) (2016) 8.
- [163] W.F. Khalik, S.-A. Ong, L.-N. Ho, Y.-S. Wong, C.-H. Voon, S.Y. Yusuf, N.A. Yusoff, S.-L. Lee, Influence of supporting electrolyte in electricity generation and degradation of organic pollutants in photocatalytic fuel cell, *Environ. Sci. Pollut. Res.* 23 (2016) 16716–16721.
- [164] D. Ying, R. Cao, C. Li, T. Tang, K. Li, H. Wang, Y. Wang, J. Jia, Study of the photocurrent in a photocatalytic fuel cell for wastewater treatment and the effects of TiO<sub>2</sub> surface morphology to the apportionment of the photocurrent, *Electrochim. Acta* 192 (2016) 319–327.
- [165] Y. Liu, L. Liu, F. Yang, Energy-efficient degradation of rhodamine B in a LED illuminated photocatalytic fuel cell with anodic Ag/AgCl/GO and cathodic ZnIn<sub>2</sub>S<sub>4</sub> catalysts, *RSC Adv.* 6 (2016) 12068–12075.
- [166] C. Hu, D. Kelm, M. Schreiner, T. Wollborn, L. Mädler, W.Y. Teoh, Designing photoelectrodes for photocatalytic fuel cells and elucidating the effects of organic substrates, *ChemSusChem* 8 (2015) 4005–4015.
- [167] D. Wang, Y. Li, G. LiPuma, Panagiotis Lianos, C. Wang, P. Wang, Photoelectrochemical cell for simultaneous electricity generation and heavy metals recovery from wastewater, *J. Hazard. Mater.* 323 (2017) 681–689.
- [168] I. Tantis, E. Stathatos, D. Mantzavinos, P. Lianos, Photoelectrocatalytic degradation of potential water pollutants in the presence of NaCl using nanocrystalline titania films, *J. Chem. Technol. Biotechnol.* 90 (2015) 1338–1344.
- [169] M. Sui, Y. Dong, H. You, Enhanced photocatalytic activity for the degradation of rhodamine B by integrating salinity gradient power into a photocatalytic fuel cell, *RSC Adv.* 5 (2015) 94184–94190.
- [170] J. Yang, W. Liao, Y. Liu, M. Murugananthan, Y. Zhang, Degradation of rhodamine B using a visible-light driven photocatalytic fuel cell, *Electrochim. Acta* 144 (2014) 7–15.
- [171] M. Antoniadou, V.M. Dascalaki, N. Balis, D.I. Kondarides, C. Kordulis, P. Lianos, Photocatalysis and photoelectrocatalysis using (CdS-ZnS)/TiO<sub>2</sub> combined photocatalysts, *Appl. Catal. B* 107 (2011) 188–196.
- [172] K.O. Iwu, A. Galekas, A.Y. Kuznetsov, T. Norby, Solid-state photoelectrochemical H<sub>2</sub> generation with gaseous reactants, *Electrochim. Acta* 97 (2013) 320–325.
- [173] B. Seger, G.Q. Lu, L. Wang, Electrical power and hydrogen production from a photo-fuel cell using formic acid and other single-carbon organics, *J. Mater. Chem.* 22 (2012) 10709–10715.
- [174] R. Bashiri, N.M. Mohamed, C.F. Kait, S. Sufian, S. Kakooei, M. Khatani, Z. Gholami, Optimization hydrogen production over visible light-driven titania supported bimetallic photocatalyst from water photosplitting in tandem photoelectrochemical cell, *Renewable Energy* 99 (2016) 960–970.
- [175] X. Liang, J. Liu, D. Zeng, C. Li, S. Chen, H. Li, Hydrogen generation promoted by photocatalytic oxidation of ascorbate and glucose at a cadmium sulfide electrode, *Electrochim. Acta* 198 (2016) 40–48.
- [176] Y. Zhang, G. Zhao, H. Shi, Y. Zhang, W. Huang, X. Huang, Z. Wu, Photoelectrocatalytic glucose oxidation to promote hydrogen production over periodically ordered TiO<sub>2</sub> nanotube arrays assembled of Pd quantum dots, *Electrochim. Acta* 174 (2015) 93–101.
- [177] H. Zhao, L. Jin, Y. Zhou, A. Bandar, Z. Fan, A.O. Govorov, Z. Mi, S. Sun, F. Rosei, A. Vomiero, Green synthesis of near infrared core/shell quantum dots for photocatalytic hydrogen production, *Nanotechnology* 27 (495405) (2016) 9.
- [178] M. Yoshii, Y. Murata, Y. Nakabayashi, T. Ikeda, M. Fujishima, H. Tada, Coverage control of CdSe quantum dots in the photodeposition on TiO<sub>2</sub> for the photoelectrochemical solar hydrogen generation, *J. Colloid Interface Sci.* 474 (2016) 34–40.
- [179] L.-C. Pop, L. Sygellou, V. Dracopoulos, K.S. Andrikopoulos, S. Sfaelou, P. Lianos, One-step electrodeposition of CdSe on nanoparticulate titania films and their use as sensitized photoanodes for photoelectrochemical hydrogen production, *Catal. Today* 252 (2015) 157–161.
- [180] L.C. Kao, S.Y.H. Liou, C.L. Dong, P.H. Yeh, C.L. Chen, Tandem structure of QD cosensitized TiO<sub>2</sub> nanorod arrays for solar light driven hydrogen generation, *ACS Sustainable Chem. Eng.* 4 (2016) 210–218.
- [181] Z. Zhang, C. Gao, Z. Wu, W. Han, Y. Wang, W. Fu, X. Li, E. Xi, Toward efficient photoelectrochemical water-splitting by using screw-like SnO<sub>2</sub> nanostructures as photoanode after being decorated with CdS quantum dots, *Nano Energy* 19 (2016) 318–327.
- [182] Z. Zhang, X. Li, C. Gao, F. Teng, Y. Wang, L.C.W. Han, Z. Zhang, E. Xie, Synthesis of cadmium sulfide quantum dot-decorated barium stannate nanowires for photoelectrochemical water splitting, *J. Mater. Chem. A* 3 (2016) 12769–12776.
- [183] S. Sfaelou, A.G. Kontos, P. Falaras, P. Lianos, Micro-Raman, photoluminescence and photocurrent studies on the photostability of quantum dot sensitized photoanodes, *J. Photochem. Photobiol. A* 275 (2014) 127–133.
- [184] P. Peerakiatkhajohn, J.H. Yun, S. Wang, L. Wang, Review of recent progress in unassisted photoelectrochemical water splitting: from material modification to configuration design, *J. Photon. Energy* 7 (2016) 012006.
- [185] C. Xiang, A.Z. Weber, S. Ardo, A. Berger, Y.K. Chen, R. Coridan, K.T. Fountaine, S. Haussener, S. Hu, R. Liu, N.S. Lewis, M.A. Modestino, M.M. Shaner, M.R. Singh, J.C. Stevens, K. Sun, K. Walczak, Modeling, simulation, and implementation of solar-driven water-splitting devices, *Angew. Chem. Int. Ed.* 55 (2016) 12974–12988.
- [186] R. Irani, N. Naseri, S. Beke, A review of 2D-based counter electrodes applied in solar-assisted Devices, *Coord. Chem. Rev.* 324 (2016) 54–81.
- [187] F. Fumagalli, S. Bellani, M. Schreier, S. Leonardi, H.C. Rojas, A. Ghadirzadeh, G. Tullii, A. Savoini, G. Marra, L. Meda, M. Grätzel, G. Lanzani, M.T. Mayer, M.R. Antognazzi, F. Di Fonzo, Hybrid organic-inorganic H<sub>2</sub> evolving photocathodes: understanding the route towards high performances organic photoelectrochemical water splitting, *J. Mater. Chem. A* 4 (2016) 2178–2187.
- [188] T. Hong, Z. Liu, X. Zheng, J. Zhang, L. Yan, Efficient photoelectrochemical water splitting over Co<sub>3</sub>O<sub>4</sub> and Co<sub>3</sub>O<sub>4</sub>/Ag composite structure, *Appl. Catal. B* 202 (2017) 454–459.
- [189] M. Haro, C. Solis, V.M. Blas-Ferrando, O. Margeat, S. Ben Dhikil, C. Videlot-Ackermann, J. Ackermann, F. Di Fonzo, A. Guerrero, S. Gimenez, Direct hydrogen evolution from Saline water reduction at neutral pH using organic photocathodes, *ChemSusChem* 9 (2016) 1–6.
- [190] E. Libnedengel Tsege, T.S. Atabaev, Md.A. Hossain, D. Lee, H.-K. Kim, Y.-H. Hwang, Cu-doped flower-like hematite nanostructures for efficient water splitting applications, *J. Phys. Chem. Solids* 98 (2016) 283–289.
- [191] H. Qi, J. Wolfe, Denis Fichou, Z. Chen, Cu<sub>2</sub>O photocathode for low bias photoelectrochemical water splitting enabled by niFe-layered double hydroxide co-catalyst, *Sci. Rep.* 6 (2016) 30882.
- [192] J. Gan, X. Lu, B.B. Rajeeva, R. Menz, Y. Tong, Y. Zheng, Efficient photoelectrochemical water oxidation over hydrogen-reduced nanoporous BiVO<sub>4</sub> with Ni-Bi electrocatalyst, *ChemElectroChem* 2 (2015) 1385–1395.
- [193] C.G. Morales-Guio, M.T. Mayer, A. Yella, S.D. Tilley, M. Grätzel, X. Hu, An optically transparent iron nickel oxide catalyst for solar water splitting, *J. Am. Chem. Soc.* 137 (2015) 9927–9936.
- [194] Z. Cai, F. Li, W. Xu, Y. Jiang, F. Luo, Y. Wang, X. Chen, Enhanced performance of photoelectrochemical water oxidation using a three-dimensional interconnected nanostructural photoanode via simultaneously harnessing charge transfer and coating with an oxygen evolution catalyst, *Nano Energy* 26 (2016) 257–266.
- [195] H. Li, Y. Qi, Z. Li, Z. Ji, X. Wu, ZnO photoanodes coated with Ni-based nanostructured electrocatalyst for water oxidation, *J. Alloys Compounds* 661 (2016) 201–205.
- [196] I.H. Kwak, H.S. Im, D.M. Jang, Y.W. Kim, K. Park, Y.R. Lim, E.H. Cha, J. Park, CoSe<sub>2</sub> and NiSe<sub>2</sub> nanocrystals as superior bifunctional catalysts for electrochemical and photoelectrochemical water splitting, *ACS Appl. Mater. Interfaces* 8 (2016) 5327–5334.
- [197] K.-Y. Yoon, H.-J. Ahn, M.-J. Kwak, S.-I. Kim, J. Park, J.-H. Jan, Selectively decorated Ti-FeOOH co-catalyst for a highly efficient porous hematite-based water splitting system, *J. Mater. Chem. A* 4 (2016) 18730–18736.
- [198] W. Li, S.W. Sheehan, D. He, Y. He, X. Yao, R.L. Grimm, G.W. Brudvig, D. Wang, Hematite-Based solar water splitting in acidic solutions: functionalization

- [199] by mono- and multilayers of iridium oxygen-evolution catalysts, *Angew. Chem. Int. Ed.* 54 (2015) 11428–11432.  
[200] P. Dias, M. Schreier, S.D. Tilley, J. Luo, J. Azevedo, L. Andrade, D. Bi, A. Hagfeldt, A. Mendes, M. Grätzel, M.T. Mayer, Transparent cuprous oxide photocathode enabling a stacked tandem cell for unbiased water splitting, *Adv. Energy Mater.* 5 (2015) 1501537.  
G. Segev, H. Dotan, K.D. Malviya, A. Kay, M.T. Mayer, M. Grätzel, A. Rothschild, High solar flux concentration water splitting with hematite ( $\alpha\text{-Fe}_2\text{O}_3$ ) photoanodes, *Adv. Energy Mater.* 6 (2016) 1500817.